

## Classical Be Stars and Classical Be Star Binaries from LAMOST DR12

QIAN-YU AN ,<sup>1</sup> WEI-MIN GU ,<sup>1</sup> AND ZHI-XIANG ZHANG ,<sup>2</sup>

<sup>1</sup>*Department of Astronomy, Xiamen University, Xiamen, Fujian 361005, People's Republic of China*

<sup>2</sup>*College of Physics and Information Engineering, Quanzhou Normal University, Quanzhou 362000, People's Republic of China*

### ABSTRACT

Classical Be (CBe) stars are rapidly rotating B-type stars with Balmer emission lines that originated from the decretion disks surrounding them in their spectra. Accounting for  $\sim 20\%$  of all B-type stars, most CBe stars are thought to form through mass and angular momentum transfer from their companions. It follows that in most close CBe star binaries, the companions are expected to be post-main-sequence stars rather than main-sequence (MS) stars. Hitherto,  $\sim 100$  CBe star binaries have been identified, the majority of which are Be/X-ray binaries. As expected, none of the others have indeed been confirmed as CBe+MS binary stars. To further study and verify the origin of CBe stars, identifying additional CBe star binaries is indispensable. In this study, we report 504 CBe stars identified using data from Data Release 12 of the Large sky Area Multi-Object fiber Spectroscopic Telescope. Among these, 141 are newly identified and 14 exhibiting radial velocity variations are identified as CBe star binaries. Besides, 60 CBe stars with high normalized unit weight error (RUWE) but not confirmed by dynamics are proposed as potential CBe star binaries. We also find that 34 CBe stars are potential cluster members. By calculating peculiar velocities, 37 runaway stars are identified with peculiar velocities ranging from  $\sim 40$  km s $^{-1}$  to  $\sim 101$  km s $^{-1}$ .

### 1. INTRODUCTION

Classical Be (CBe) stars are rapidly rotating B-type stars with Balmer emission lines that originated from the decretion disks surrounding them (e.g. J. M. Porter & T. Rivinius 2003; T. Rivinius et al. 2013). The rotational velocities of CBe stars can be up to more than 0.7 times their critical rotation velocities (e.g. T. Rivinius et al. 2013; J. Zorec et al. 2016) and various channels have been proposed to explain why they rotate rapidly.

P. Bodenheimer (1995) advocated that certain B-type stars are endowed with a substantial amount of angular momentum inherited from their parent molecular clouds, causing them to be fast rotators right from their formation, ultimately becoming CBe stars. However, some studies on open clusters suggested that Be stars are not only young stars, but in all ages (H. A. Abt 1979; J. C. Mermilliod 1982; A. Slettebak 1985). Moreover, it has been shown that most young B stars have rotational velocities that are well below the limit for Be star formation (S. C. Wolff et al. 2004; W. Huang et al. 2010).

Another single star evolution channel that forms CBe stars is angular momentum transfer from the core to the envelope to accelerate B stars (e.g. S. Ekström et al. 2008; A. Granada et al. 2013; B. Hastings et al. 2020). On the other hand, B. Hastings et al. (2020) also pointed out that CBe stars formed through such a channel should have much larger surface nitrogen enhancement, while only a small portion of CBe stars exhibit the model prediction of nitrogen enrichment (P. R. Dunstall et al. 2011).

Single star evolution channel does not seem to dominate the formation of CBe stars, implying the existence of alternative formation channels. The binary interaction channel proposes that a star can be spun up through mass and angular momentum transfer from an evolved companion (e.g. S. Kriz & P. Harmanec 1975; O. R. Pols et al. 1991). Supporting this, M. V. McSwain & D. R. Gies (2005) conducted a photometric survey of 55 southern open clusters and concluded that up to 73% of Be stars may have been spun up via binary mass transfer. Later, Y. Shao & X.-D. Li (2014) provided theoretical support using the BSE code (J. R. Hurley et al. 2002), demonstrating that most Be

stars likely originate from binary interactions. Consequently, if a companion of a CBe star survives from the binary interactions, it should be a post-main-sequence object, such as an O/B-type hot subdwarf (sdO/B), a stripped helium star, or a compact object, rather than a main-sequence star.

There is no doubt that searching for more CBe stars and CBe star binaries is necessary to further study and verify the origin of CBe stars. Since the first identification of CBe star,  $\gamma$  Cas, also the first star found to show emission lines in the spectrum (A. Secchi 1866), thousands of CBe stars have been identified by numerous photometric or spectroscopic measurements (e.g. S. D. Chojnowski et al. 2015; C.-C. Lin et al. 2015; W. Hou et al. 2016) and compiling of the CBe star catalogs has also been carried out accordingly (e.g. M. Jaschek & D. Egret 1982; C. Neiner et al. 2011). Among them, the Be Star Spectra database established by C. Neiner et al. (2011) is not only a catalog but also a collection of 323,030 spectra for 2,455 Be stars as of June 18, 2025. Additionally, optical counterparts of several X-ray sources have been identified as CBe stars (e.g. P. Reig & P. Roche 1999; J. A. Tomsick et al. 2011), expanding both the known population of CBe stars and Be/X-ray binaries. In Be/X-ray binaries, all the confirmed companions in the Milky Way are neutron stars, while several cases for white dwarf companions have been found in the Large Magellanic Cloud and Small Magellanic Cloud (e.g. P. Kahabka et al. 2006; J. A. Kennea et al. 2021; A. Marino et al. 2025). Meanwhile, progress has also been made in identifying Non-X-ray source CBe binaries based on the CBe star samples, with most confirmed companions in these systems being sdO/Bs (e.g. G. J. Peters 1983; L. B. F. M. Waters et al. 1991; L. Wang et al. 2018, 2021; S. Nedhath et al. 2025). Rarely, several CBe stars were found or suspected to reside in triple systems, e.g., V1371 Tau (T. Rivinius et al. 2025; D. F. Rocha et al. 2025),  $\nu$  Gem (R. Klement et al. 2021),  $\delta$  Sco (A. S. Miroshnichenko et al. 2013) and 60 Cyg (R. Klement et al. 2022). Evidence or hints for multiplicity in these systems has primarily been obtained through orbital analysis, long-term RV monitoring, as well as high-angular-resolution techniques such as speckle observations and interferometry observations.

In this work, we report the identification of 504 CBe stars (141 newly identified) from the Data Release 12 (DR12) of the Large Sky Area Multi-Object Fiber Spectroscopy Telescope (LAMOST), of which 14 exhibit radial velocity (RV) variations. The structure of this paper is organized as follows. We introduce the spectra collected in Section 2. In Section 3, we describe the process of selecting CBe stars. In Section 4, we present 14 CBe star binaries identified in this work and attach 60 potential CBe star binaries. In Section 5, we study the spatial distribution of these CBe stars and identify potential cluster members and runaway stars among them. We summarize our results and make a discussion in Section 6.

## 2. LAMOST SPECTRAL OBSERVATION

LAMOST, also known as the GuoShouJing Telescope, is a special 4-meter aperture reflecting Schmidt telescope with an installment of 4,000 fibers within the 5 deg field of view (X.-Q. Cui et al. 2012), thus possessing extremely high spectral acquisition efficiency. It launched the first five-year survey with low-resolution spectrographs ( $R = 1,800$ ) since 2012 (A. L. Luo et al. 2015), later expanding to include medium-resolution spectrographs ( $R = 7,500$ ) in 2017 (C. Liu et al. 2020). The low-resolution spectra cover a broad wavelength range of 3,700 Å to 9,000 Å, while the medium-resolution spectra cover wavelength ranges from 4,950 Å to 5,350 Å and 6,300 Å to 6,800 Å for the blue arms and the red arms, respectively. For stars with spectral type late A, F, G, K, or M, stellar parameters are derived using the LAMOST Stellar Parameter Pipeline (A. L. Luo et al. 2015, 2018; B. Du et al. 2021). However, for hotter stars, only spectral classifications are available in low-resolution spectra, while neither stellar parameters nor spectral classifications are available for hot stars in medium-resolution spectra.

As of DR12, LAMOST has collected an impressive total of 12,602,390 low-resolution spectra (LRS) and 15,475,985 medium-resolution spectra<sup>3</sup> (MRS), representing one of the largest stellar spectroscopic databases available. Among them, 12,110,344 medium-resolution spectra belong to time-domain survey (S. Wang et al. 2021); therefore, numerous sources have multi-epoch spectra, which can be used for RV monitoring and search for binaries.

Our initial sample contains 14,981 sources classified as O/B-type stars (`subclass:B, B6, B9, O or OB`) in at least one low-resolution spectral observation. After cross-matching these sources with the medium-resolution database, we finally obtain a total of 34,558 LRS and 25,809 MRS corresponding to these sources.

<sup>3</sup> <https://www.lamost.org/dr12/>

### 3. SAMPLE SELECTING

#### 3.1. Preliminary selection of CBe stars by checking spectra

We inspect the obtained spectra of the initial sample by eye-checking and apply the following two criteria to select CBe stars preliminarily:

1. The H $\alpha$  exhibits a strong emission line (with a full width  $> 5 \text{ \AA}$  in MRS or  $> 10 \text{ \AA}$  in LRS, respectively) in at least one spectrum,
2. There are no forbidden emission lines such as [O III]  $\lambda 4959, \lambda 5007$ , [N II]  $\lambda 6583$  and [S II]  $\lambda 6717, \lambda 6731$  in the spectra.

The second criterion excludes Herbig Ae (HAe) or Be (HBe) stars and sources located in the H II regions. While these sources exhibit H $\alpha$  emission similar to CBe stars, they can be distinguished by their additional forbidden line emission - a characteristic feature of low-density environments. In contrast, CBe stars possess high-density circumstellar disks that preclude forbidden line emission. Applying these two criteria yields a preliminarily sample of 538 CBe star candidates.

#### 3.2. Cross-matching with known CBe star catalogs

Building upon the preliminary sample selection described in Section 3.1, we cross-match it with the available CBe star catalogs compiled by M. Jaschek & D. Egret (1982); C. Neiner et al. (2011); S. D. Chojnowski et al. (2015); C.-C. Lin et al. (2015); P. S. Chen et al. (2016); W. Hou et al. (2016); M. Vioque et al. (2020); B. Shridharan et al. (2021) and L. Wang et al. (2022). This cross-matching serves two purposes: (i) to quantify the number of newly identified CBe stars in our sample, and (ii) to eliminate misclassified or controversial sources in our sample. Besides, we also retrieve the SIMBAD database (M. Wenger et al. 2000) to obtain the main type and other types and record whether they contain ‘Be’ to supplement the missing sources in the above catalogs. Following this cross-matching procedure, we identify 24 sources requiring exclusion: 12 show conflicting classifications as a CBe star and other types (evolved, [H II], HBe star or B[e]) in different sources, while another 12 are never classified as CBe stars in any available catalog. After removing these sources, 514 sources are reserved, including 147 newly identified sources.

#### 3.3. IR test

To further remove HAe/HBe stars from the sample and strengthen the accuracy of the sample as much as possible, we perform the IR test, suggested by the fact that the IR excess in HAe/HBe stars is stronger than that of CBe stars (U. Finkenzeller & R. Mundt 1984). We identified HAe/HBe stars by applying a modified, more stringent version of the criterion established by W. Hou et al. (2016):  $H - K > 0.4$  or  $K - W_1 > 0.8$ , where  $H$ ,  $K$  and  $W_1$  are the  $H$  band of 2MASS (M. F. Skrutskie et al. 2006), the  $K_s$  band of 2MASS and the  $W_1$  band of WISE (E. L. Wright et al. 2010), respectively. We retrieve photometric data of 2MASS and WISE respectively from II/246/out (R. M. Cutri et al. 2003) and II/328/allwise (R. M. Cutri et al. 2021) of Vizier catalogs (F. Ochsenbein et al. 2000). To correct for interstellar extinction, we obtain extinction values from GALEXtin<sup>4</sup> (E. B. Amôres et al. 2021), using the model constructed by G. M. Green et al. (2019). The distances required for this process are taken from C. A. L. Bailer-Jones et al. (2021). Following the reddening law of J. A. Cardelli et al. (1989) with  $R_V = 3.1$ , we convert the extinction values into the color excess of  $E(H - K)$  and  $E(K - W_1)$  using the wavelength-dependent extinction ratios from VOSA<sup>5</sup> (A. Bayo et al. 2008). After applying these corrections, we calculate de-reddened  $H - K$  and  $K - W_1$ , identifying 505 CBe stars, including 142 newly identified sources.

#### 3.4. Stellar properties

To investigate the stellar properties of these CBe stars, we plot them on the Hertzsprung–Russell diagram (HRD) and cross-match their LAMOST/LRS spectra with high signal-to-noise ratio (SNR) with observed spectra of other B stars with spectral classification.

We take 400,000 stars from *Gaia* DR3 as the background of HRD, selected by the following criteria:

1. Parallax  $> 2 \text{ mas}$  and parallax\_over\_err  $> 10$ ,

<sup>4</sup> <http://galexint.org/>

<sup>5</sup> <http://svo2.cab.inta-csic.es/theory/fps/>

2. `|Galactic latitude| > 30,`
3. `RUWE < 1.4,`
4. `phot_g_mean_flux_over_error > 50,`
5. `phot_rp_mean_flux_over_error > 20,`
6. `phot_bp_mean_flux_over_error > 20,`
7. `1.0 + 0.015 * power(phot_bp_mean_mag - phot_rp_mean_mag, 2) < phot_bp_rp_excess_factor < 1.3 + 0.060 * power(phot_bp_mean_mag - phot_rp_mean_mag, 2),`
8. `visibility_periods_used > 8.`

We then select 475 sources with relative distance uncertainty not exceeding 20% to calculate their de-reddened absolute  $G_{\text{mag}}$  and BP - RP, following the similar method as described in Section 3.3, and plot them on the HRD (see Figure 1). Most sources in our sample lie on or near the main sequence, and none occupies the subdwarf region. Two objects—J063809.24+034454.6 (marked by an aquamarine dot in Figure 1) and J033630.81+480913.2 (marked by an orange dot in Figure 1)—appear as outliers with significantly redder BP - RP colors. Inspection of their spectra reveals strong Ca II triplet absorption line but no He I absorption lines in J033630.81+480913.2, indicating an F-type (or later-type) star. Although there is only one spectrum with low SNR (< 30 across most wavelength ranges) for J033630.81+480913.2, preventing an in-depth analysis of it, we exclude J033630.81+480913.2 from our CBe star sample to ensure a purer sample. In contrast, J063809.24+034454.6 is confirmed to be a B-type star based on the presence of Balmer series, He I lines, and Paschen series in its spectrum. However, its blue-arm flux is substantially lower than that of the medium-arm, implying unusually strong interstellar extinction. This extinction is likely underestimated by the universal model, leading to a severely overestimated de-reddened BP - RP color. Ultimately, we identify 504 CBe stars, including 141 newly identified sources. In Tables 1 and 2, we list these 504 identified CBe stars and 33 sources excluded by Section 3.2 and 3.3, respectively.

We also derive the spectral types and luminosity classes of 405 sources in our sample by matching their optical spectra with the spectral library of B-type MK standard stars. These 405 sources satisfy the requirement of having at least one LAMOST/LRS spectrum with a SNR in the  $g$  band of  $\geq 40$ . For sources with multiple spectra meeting this criterion, we consistently adopt the spectrum with the highest SNR. The spectra of B-type MK standard stars are obtained from the IACOB project, which has developed a new grid of northern standards for the spectral classification of more than 150 B-type stars and four A-type stars (I. Negueruela et al. 2024). This grid covers the classical classification spectral range from 3,900 Å to 5,100 Å with spectral resolution of  $\sim 4,000$ . For consistency, we degrade the spectra of B-type MK standard stars to 1,800 to match the spectral resolution of LAMOST/LRS spectra. Furthermore, to minimize the effects caused by the differences of RVs and projected rotational velocities between the standard stars and our sample, we apply a systematic grid of RVs and  $V_{\text{sin}i}$  to the LAMOST/LRS spectra of our sample in the matching process. The grids explore RVs and  $V_{\text{sin}i}$ s ranging from -100 to 100 km s $^{-1}$  and from 50 km s $^{-1}$  to 410 km s $^{-1}$ , with steps of 10 km s $^{-1}$  and 20 km s $^{-1}$ , respectively.

We identify the match with minimal  $\chi^2/N$  as the best match for each source. The  $\chi^2/N$  is defined as:

$$\chi^2/N = \frac{1}{N} \sum_i \left( \frac{f_{\text{obs}}^i - f_{\text{lib}}^i}{f_{\text{err}}^i} \right)^2,$$

where  $f_{\text{obs}}^i$  refers to the flux of the LAMOST/LRS spectrum of a given source at wavelength  $i$ ,  $f_{\text{lib}}^i$  refers to the flux of a spectrum of standard star at wavelength  $i$ ,  $f_{\text{err}}^i$  refers to the observed uncertainty of flux at wavelength  $i$ , and  $N$  is the number of wavelength points. During the calculation of  $\chi^2/N$ , we select the spectral range from 4,000 Å to 4,800 Å, masking the Balmer series and the diffuse interstellar bands. There are no O-type standard stars, so potential Oe stars in our sample will be misclassified. Considering the rarity of O-type stars, it will not cause significant impact. In Table 3, we show the best matches for sources with  $\chi^2/N \leq 9$  and  $\sim 90\%$  of them are with luminosity classes of III, IV or V.

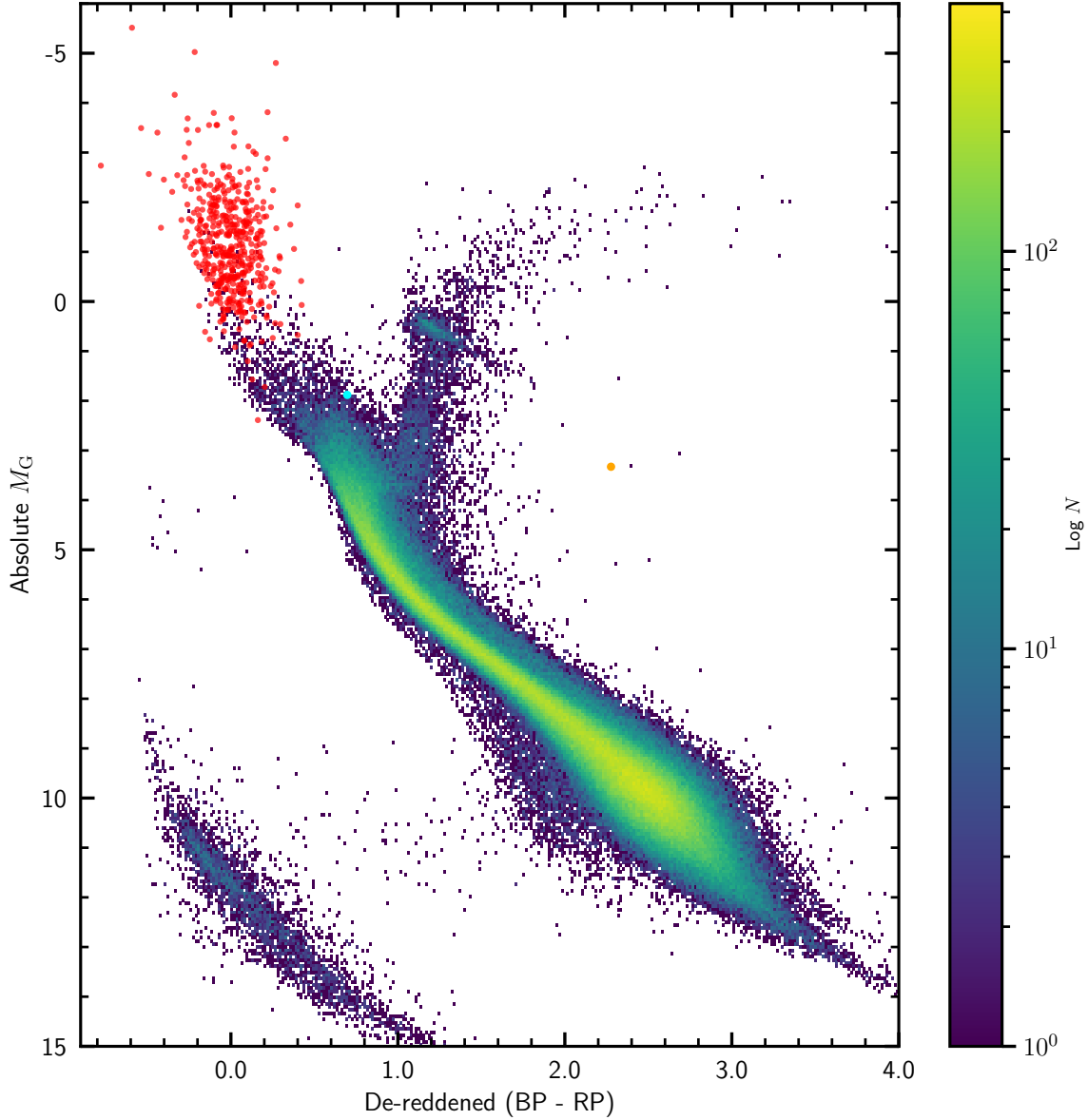


**Figure 1. The distribution of CBe stars in our sample on the HRD.** Most sources in our sample are marked by red dots, while two outliers, J033630.81+480913.2 and J063809.24+034454.6, are marked by an orange dot and an aquamarine dot, respectively.

#### 4. CBe STAR BINARIES

##### 4.1. Identified CBe star binaries

Each of the 504 CBe stars in our sample has been observed by LAMOST an average of 6.2 times, enabling monitoring of their RV variations. Figure 2 shows the distribution of the number of observations for these sources. To identify CBe stars with significant RV variations, we preselect 14 sources exhibiting visible spectral line shifts through visual inspection. We then apply the criterion from H. Sana et al. (2013) to solidify the result — a source is classified as RV-variable if at least one pair of its RV measurements simultaneously satisfies the following equations:

$$\sigma_{\text{detect}} = \frac{|v_i - v_j|}{\sqrt{\sigma_i^2 + \sigma_j^2}} > 4.0 \quad \text{and} \quad |v_i - v_j| > C, \quad (1)$$

**Table 1.** CBe stars identified from LAMOST DR12

LAMOST designation	Simbad name	Gaia DR3 ID	R.A. (deg)	Decl. (deg)	New CBe star?
J000003.86+635429.6	EM* VES 976	431630851621447552	0.016093	63.908246	No
J000305.76+632002.1	—	431579342069149184	0.774036	63.33392	Yes
J000336.71+635514.3	—	431622845802749696	0.902974	63.92066	Yes
J000352.84+573550.0	—	422602452401685120	0.970206	57.597233	No
J000429.45+644140.6	LS I +64 14	432136141624375808	1.122739	64.694625	Yes
...	...	...	...	...	...

**Notes.** The complete table is available in the online journal and at CDS.

where  $v_i$  and  $\sigma_i$  are the RVs and their  $1\sigma$  errors at epoch  $i$ , and  $C$  is the minimum amplitude threshold. [H. Sana et al. \(2013\)](#) adopted  $C = 20 \text{ km s}^{-1}$ . These two criteria have been carried forward by many following studies on massive-star multiplicity (e.g. [J. Bodensteiner et al. 2021](#); [G. Banyard et al. 2022](#); [J. I. Villaseñor et al. 2025](#)). All of these preselected 15 sources satisfy the second criterion in Eq. 1. We measure RVs of these preselected sources mainly using He I 6678 absorption line. For those with a He I 6678 absorption line unavailable (may be due to low SNR or high variation), the He I 4922 absorption line or the wing of the H $\alpha$  emission line (the part below half of the maximum height of the H $\alpha$  emission line) could be a substitute. We employ Gauss-like model to fit the profiles of selected spectral lines to determine their centers and convert the shifts of the centers from the wavelength of the specific lines under a rest frame into RVs by the following equations:

$$F_\lambda = h \pm \frac{A}{\sqrt{2\pi}\sigma} \exp^{\frac{-(\lambda - \lambda_c)^2}{2\sigma^2}} \text{ (“+” for H}\alpha\text{ emission line and “-” for absorption line)} \text{ and } RV = \frac{\lambda_c - \lambda_{\text{rest}}}{\lambda_{\text{rest}}} c, \quad (2)$$

where  $F_\lambda$  denotes the normalized flux;  $h$  is approximately 1, representing the local continuum;  $\lambda_c$  is the central wavelength;  $A$  is a factor to adjust the contour longitudinally;  $\sigma$  is the standard deviation;  $\lambda_{\text{rest}}$  is the wavelength of the specific absorption lines under a rest frame; and  $c$  is the speed of light in vacuum. We execute `emcee` ([D. Foreman-Mackey et al. 2013](#)) with 24 walkers, taking 10,000 steps per walker to sample the parameter space. The initial 5,000 steps of each walker are regarded as the burn-in and consequently discarded. For each parameter, we take the 50<sup>th</sup> percentile, 15.87<sup>th</sup> percentile and 84.13<sup>th</sup> percentile of the posterior distribution as the best-fit value, the  $1\sigma$  lower limit and the  $1\sigma$  upper limit, respectively. Particularly, LAMOST J045300.92+291405.2 displays a distinctive spectral feature: prominent Fe and Mg absorption lines where emission lines typically appear for CBe stars, particularly among early-type ones, and we measure RVs of it by the cross-correlation function technique ([J. Tonry & M. Davis 1979](#)) using the blue arms of LAMOST/MRS spectra.

Among the preselected 15 sources, one source, LAMOST J010906.43+562643.1 fails to satisfy the first criterion in Eq. 1 and is therefore excluded from the final sample. Of the identified 14 RV-variable systems: Five are newly identified CBe stars in this study, and one, ALS 8814, was previously reported as a CBe star + black hole (BH) binary candidate ([Q.-Y. An et al. 2025](#)), but [K. El-Badry et al. \(2025\)](#) argued that the companion in ALS 8814 is a visible star by their spectral disentangling. For each of the 13 newly identified CBe star binaries, we list them in Table 4. Figure 3 displays two spectra corresponding to the epochs of maximum RV separation for each newly identified CBe star binary.

#### 4.1.1. Two astrometric binaries in Gaia DR3

Within our sample of 14 newly identified CBe star binaries, two systems are classified as astrometric binaries (`non_single_star != 0`) in Gaia DR3 ([Gaia Collaboration et al. 2023](#)). One source, LAMOST J045300.92+291405.2, whose `nss_solution type` is single-line spectroscopic binary (SB1), has an astrometric published orbital solution in the `gaiadr3.nss_two_body_orbit` catalog, with an orbital period of  $67.82 \pm 0.56$  days, a RV semi-amplitude of  $14.67 \pm 2.81 \text{ km s}^{-1}$  and an orbital eccentricity of  $0.34 \pm 0.13$ . The RV semi-amplitude reported in `gaiadr3.nss_two_body_orbit` catalog is consistent with that observed in the available LAMOST spectra (see Figure 3). The other source, LAMOST J060547.24+220818.7, has a `nss_solution type` of First Degree Trend SB1. While no orbital solution is available, *Gaia*

**Table 2.** 33 sources excluded by cross-matching with known CBe star catalogs and IR test

LAMOST designation	<i>Gaia</i> DR3 ID	R.A. (deg)	Decl. (deg)	Excluded by	Other type(s) [Ref.]	H - K (mag)	K - W <sub>1</sub> (mag)
J015650.77+574037.6	505371935395794432	29.211578	57.677124	Cross-matching	Evolved [3]	0.14	0.23
J034158.92+575733.6	449123153896296704	55.4955	57.959361	IR test		-0.08	1.37
J035952.32+481339.9	246810265606108544	59.968015	48.227753	Cross-matching	HBe [3]	-0.03	1.18
J041805.77+533707.2	275377398760016000	64.524051	53.618671	Cross-matching	HBe [3]	-0.05	0.97
J042118.65+451430.8	232751566334445568	65.32773	45.241901	Cross-matching	A[e] [3]	-0.01	0.14
J043000.64+422259.6	252274593578484992	67.502696	42.383247	Cross-matching	HBe [3]	-0.05	1.25
J043638.32+545049.5	274087843419934208	69.159697	54.847097	Cross-matching	HII [1]	0.04	0.07
J044531.85+544316.3	274177694136042496	71.382746	54.721206	IR test		-0.06	0.88
J050104.85+262444.2	3420337681942539520	75.270218	26.412281	IR test		-0.10	0.89
J051838.65+350814.2	183624252932329728	79.661056	35.137287	Cross-matching	HII [1]	-0.02	0.01
J052019.20+320817.0	180790154334589696	80.08001	32.138056	Cross-matching	HII [1]; HBe [3]	-0.01	0.98
J052958.80+330642.2	3449029781465926400	82.495015	33.111744	Cross-matching	HII [1]	0.00	0.08
J053123.44+383157.2	190415420860586624	82.847667	38.532583	Cross-matching	PMSc [2]	0.23	0.76
J053141.10+091327.9	3337843940146649984	82.921254	9.22443	Cross-matching	HII [1]	0.19	-0.05
J053201.66+363519.2	183489867698309888	83.006942	36.588679	IR test		-0.04	1.02
J053304.40+300057.1	3446048597423458432	83.268348	30.015879	Cross-matching	B[e] [3]	0.10	0.08
J053308.45+261924.4	3441911547485643136	83.285249	26.323461	IR test		-0.05	1.13
J053309.04+291103.0	3445858794228638592	83.287708	29.184194	IR test		0.03	0.81
J054443.01+263002.0	3441355396462179456	86.179232	26.500569	Cross-matching	B[e] [3]	0.07	-0.10
J054848.25+283547.7	3443142313313938816	87.201083	28.596611	Cross-matching	B[e] [3]	0.13	0.12
J055554.65+284706.3	3431561569657351936	88.977746	28.785103	IR test		-0.01	2.03
J055838.98+201108.5	3422833371476299264	89.662417	20.185722	Cross-matching	HBe [1,3]; PMSc [2]	0.76	1.07
J060147.79+404022.4	3458471704427619456	90.44915	40.67291	Cross-matching	B[e] [3]	0.08	-0.01
J060414.76+240402.4	3426211861471165952	91.061522	24.067347	Cross-matching	HBe [3]	0.00	1.02
J062029.71+040604.6	3125446193770750976	95.123809	4.101283	Cross-matching	HBe [3]	-0.02	0.91
J062531.59+200550.4	3372586102405306496	96.381646	20.097346	Cross-matching	Evolved [3]	0.15	0.54
J064056.90+115646.4	3352022383108018176	100.23712	11.946228	Cross-matching	HII [1]	0.14	0.22
J064409.32+112626.8	3351184898843187072	101.03887	11.440784	Cross-matching	HII [1]	0.03	-0.03
J065910.35-003708.4	3112643823976115072	104.793129	-0.619007	IR test		0.23	3.74
J074409.19+020131.1	3088632444230894592	116.03831	2.025315	IR test		0.05	2.36
J213341.54+415208.5	1967510469468468096	323.4231	41.86905	Cross-matching	Evolved [3]	0.18	0.37
J214356.11+390537.4	1954023035205245312	325.983794	39.093748	Cross-matching	HII [1]	—	—
J224515.96+563739.7	2006972762119220480	341.316504	56.627719	Cross-matching	HBe [3]	0.05	1.01

HII: Spectra contaminated by HII regions.

PMSc: Pre-main sequence candidates.

Reference: [1] [W. Hou et al. \(2016\)](#); [2] [M. Vioque et al. \(2020\)](#); [3] [B. Shridharan et al. \(2021\)](#).

DR3 reports a `rv_amplitude_robust` (total amplitude in the RV time series after outlier removal) of 125.99 km s<sup>-1</sup>, exceeding the maximum RV separation observed in the available LAMOST spectra.

#### 4.1.2. Other 12 newly identified CBe star binaries

The other 12 newly identified CBe star binaries show maximum RV separations ranging from  $\sim$ 20 km s<sup>-1</sup> to  $\sim$ 130 km s<sup>-1</sup> in available LAMOST spectra.

**Table 3.** Spectral match results of sources with spectra of high SNR

LAMOST designation	<i>Gaia</i> DR3 ID	SNR ( <i>g</i> band)	Best-matched standard star	Spectral type	Luminosity	$\chi^2/N$
J000003.86+635429.6	431630851621447552	207.76	HD 144470	B1	V	7.53
J000305.76+632002.1	431579342069149184	80.78	HD 35299	B1.5	V	7.95
J000336.71+635514.3	431622845802749696	161.67	HD 34503	B6	III	5.04
J000352.84+573550.0	422602452401685120	165.31	HD 207330	B2.5	III	1.61
J000429.45+644140.6	432136141624375808	156.31	HD 21483	B3	III	6.21
...	...	...	...	...	...	...

**Notes.** The complete table is available in the online journal and at CDS.

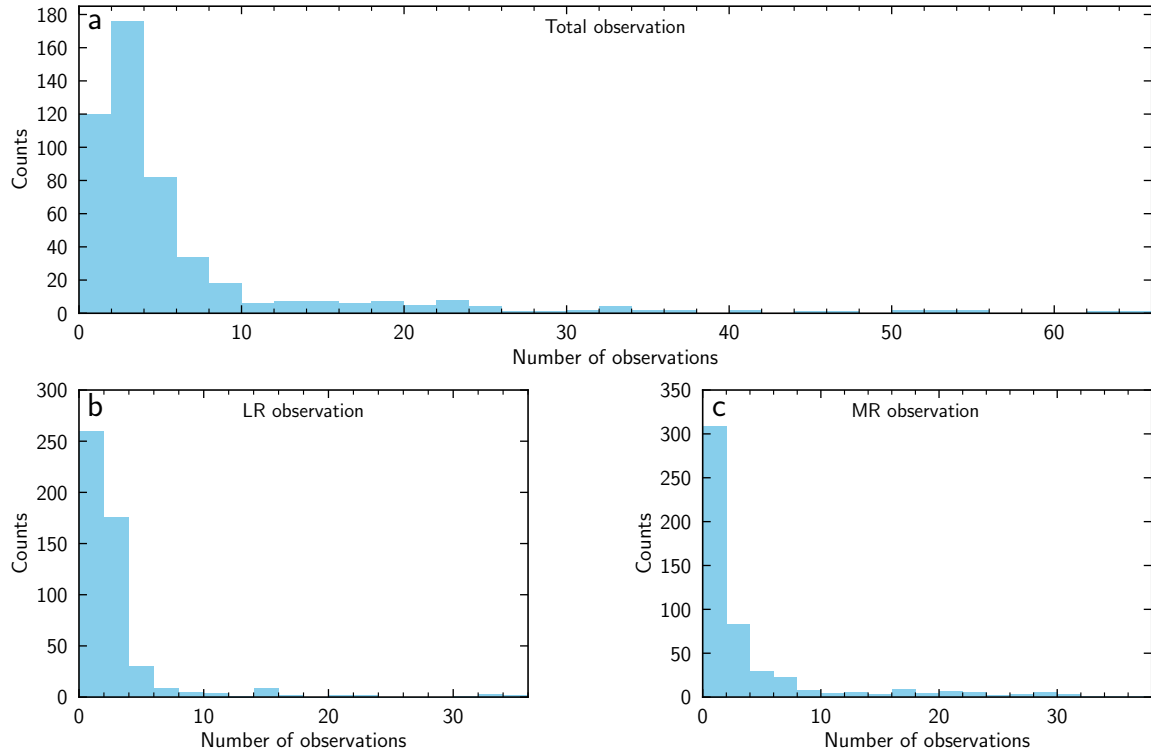


**Figure 2.** **a**, Distribution of total number of observations of the 504 CBe stars in LAMOST. **b**, Distribution of number of observations of the 504 CBe stars in low-resolution survey of LAMOST. **c**, Distribution of number of observations of the 504 CBe stars in medium-resolution survey of LAMOST.

Among these systems, LAMOST J035933.84+555751.1 stands out with a maximum RV separation of  $\sim 130 \text{ km s}^{-1}$ , higher than that of any known CBe star binaries. Its sole LAMOST/LRS spectrum reveals a He II 4686 absorption line, indicative of a hot component ( $T_{\text{eff}} > 30,000 \text{ K}$ ). It is meaningful to discuss whether it originated from the CBe star itself or a potential hot companion. We measure the RVs of He II 4686 absorption line and He I 6678 absorption line, and obtain  $-10.08^{+6.59}_{-6.65} \text{ km s}^{-1}$  and  $6.08^{+3.71}_{-3.73} \text{ km s}^{-1}$ , respectively (see Figure 4). The  $\sigma_{\text{detect}}$  of this set of measurements is 2.13, which is lower than the threshold for significant differences defined by Eq. 1. However, even if there is no significant RV difference between these two lines, it is not enough to definitively establish a shared stellar origin of these two lines, as the single-epoch spectrum may be obtained (nearly) at the superior conjunction or inferior

**Table 4.** 13 newly identified CBe star binaries from LAMOST DR12

LAMOST designation	<i>Gaia</i> DR3 ID	R.A. (deg)	Decl. (deg)	N	$\Delta RV^1$	$\sigma_{\text{detect}}$	RUWE	New	Notes
								CBe star?	
J035933.84+555751.1	468716416747466752	59.891003	55.964199	12	128.56	49.61	10.32	Yes	
J040251.79+470329.0	245895639429336064	60.715833	47.058073	8	82.42	5.41	1.23	No	H $\alpha$ emission line seems stationary
J060547.24+220818.7	3423721944373852672	91.446842	22.13855	47	63.04	13.67	0.97	No	Astrometric binary; H $\alpha$ emission line seems stationary
J070548.10+263603.6	883218724017482880	106.450446	26.601008	5	61.31	9.78	0.96	No	
J025812.40+534150.1	441310466646282880	44.551677	53.697273	28	55.90	23.25	0.96	No	
J061116.79+232521.8	3425411417005784448	92.81998	23.422722	62	45.95	20.47	1.15	No	
J061202.17+211717.5	3375360788715959552	93.009069	21.288215	45	45.41	23.95	10.80	No	
J065728.90+075920.0	3157092612318301696	104.370421	7.988902	5	44.58	80.17	0.91	Yes	
J045558.23+422925.4	204958970401866624	73.99264	42.490414	4	42.29	5.77	1.21	No	
J063326.66-000430.1	3119304940291183744	98.361086	-0.075046	3	32.21	11.43	0.98	Yes	
J055339.78+284729.6	3443195399110392192	88.415758	28.791573	31	30.98	230.27	1.82	No	
J045300.92+291405.2	155287742339368448	73.253872	29.234795	8	29.61	987.00	1.13	Yes	Astrometric binary
J025158.41+570147.2	460613256564267008	42.993397	57.029804	11	22.35	20.24	3.39	No	

<sup>1</sup>: Maximum RV separation observed in LAMOST spectra (km s<sup>-1</sup>).

conjunction. Unfortunately, LAMOST/MRS spectra lack He II 4686 coverage, making it unable to chronically track its movement in available data.

We also attempt to identify its spectral type by matching spectral characteristics using stellar observational spectra in [J. Maíz Apellániz et al. \(2026\)](#). The strong Ca II is 3934 line indicate that the spectral type of LAMOST J035933.84+555751.1 is not later than O9, while the non-weak He I lines and the absence of N III 4634/41/42 emission lines excludes a spectral type of earlier than or equal to O7 (see Figure 5). Though B-type (super)giants also exhibit the above features, they also exhibit strong Si III 4553/4568/4575 absorption lines, inconsistent with that of LAMOST J035933.84+555751.1. Therefore, we identify LAMOST J035933.84+555751.1 as an O8-O9 star.

In summary, we incline to the view that LAMOST J035933.84+555751.1 is actually an Oe star with spectral type of O8-09 and the He II 4686 absorption line originates from the Oe star itself. Besides, LAMOST J035933.84+555751.1 is a source warranting follow-up observations because of its huge RUWE (see Table 4), which may hint a wide orbit and consequently a long orbital period. Significant RV variation and long orbital period will yield a high mass function, indicative of a heavy companion (possibly neutron star or BH).

#### 4.2. Other potential CBe star binaries

RUWE provided by *Gaia* is an excellent indicator of wide binary systems, particularly when long-term RV monitoring is unavailable. RUWE quantifies the deviation of a source's astrometric observations from the best-fitting single-star model. For sources with well-behaved astrometric solutions, RUWE is expected to be close to  $\sim 1$  (see [https://dms.cosmos.esa.int/COSMOS/doc\\_fetch.php?id=3757412](https://dms.cosmos.esa.int/COSMOS/doc_fetch.php?id=3757412)). For a star, a common scenario resulting in a RUWE significantly greater than 1 (e.g., RUWE  $> 1.4$ ) is the presence of an unresolved, dim companion orbiting at a wide separation. The orbital motion induced by the companion, which is not accounted for in the single-star model, causes the observed motion to be poorly fitted. RUWE exhibits a specific dependence on the orbital period and the projected semi-major axis. It initially increases with the orbital period and the projected semi-major axis. However, for orbital periods exceeding approximately  $\sim 1,000$  days, RUWE begins to decrease due to the finite five-year baseline of *Gaia* observations, which is insufficient to resolve very long-period orbits fully. Based on this theory, [Gaia Collaboration et al. \(2024\)](#) identified a binary comprising a G9/K0-type star and a  $33 M_{\odot}$  BH in an 11.6-year orbit while validating the preliminary *Gaia* astrometric binary solutions. Furthermore, [P. Nagarajan et al. \(2025\)](#) initiated a large-scale search for dormant BHs in wide binaries by combining spectroscopic follow-up on a sample of low-metallicity stars with

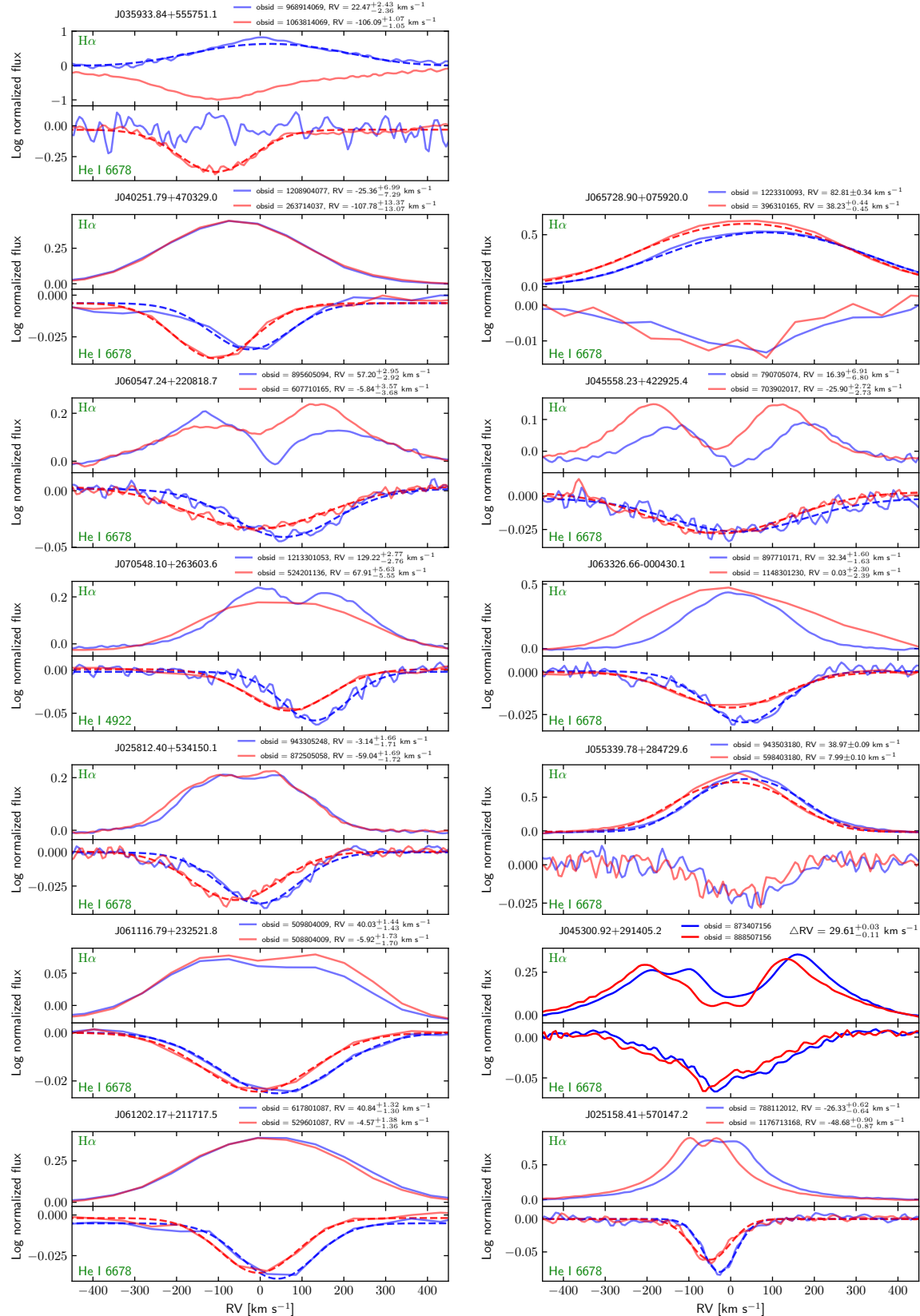


**Figure 3.** The two spectra with maximum RV separation for each 13 newly identified CBe star binaries. Spectra are plotted by light solid lines, while model lines are plotted by dark dashed lines. To strengthen the visual contrast, we plot the logarithm of all the fluxes and the spectrum with obsid of 1063814069 (belongs to J035933.84+555751.1) is amplified by a factor of 7.

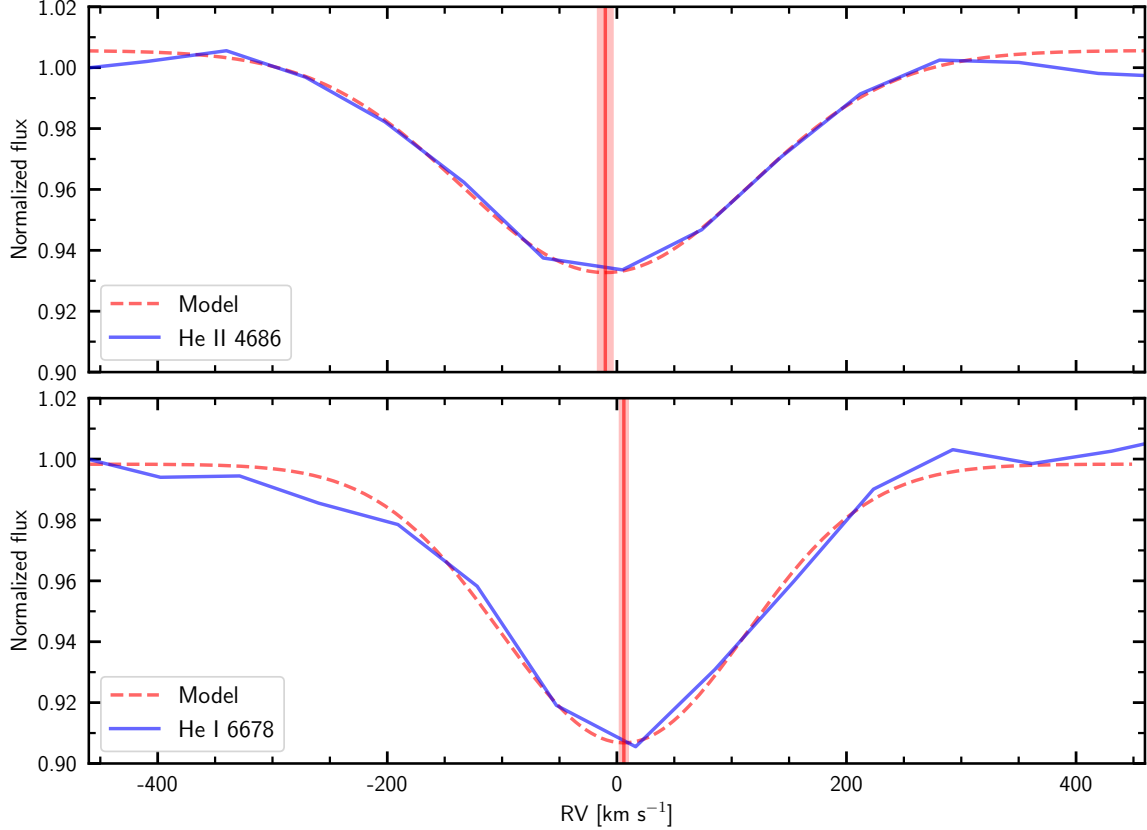


**Figure 4.** The contrast of RVs measured by He II 4686 line and He I 6678 line of LAMOST 035933.84+555751.1. We convert wavelengths into RV space and the RV zero points for He II 4686 line and He I 6678 line are 4686.98 Å and 6680 Å, respectively. In both panels, we use solid blue lines and red dashed lines to represent spectra and best-fit model lines, respectively. The vertical red lines show the measured RVs and the light red shaded areas reflect the  $1\sigma$  uncertainties.

acceleration solutions or high RUWE, yielding several promising sources. Thus it can be seen that high RUWE is indeed a wonderful indicator of wide binaries in practice.

Of the CBe stars in our sample, 60 exhibit a RUWE exceeding 1.4, and 38 have a RUWE greater than 2.0. Among these, five and four sources, respectively, show RV variations reported in Section 4.1. In addition, *Gaia* DR3 also reported four RV-variable sources and three RV-variable sources, respectively, for these two RUWE-threshold standards. All of the four sources do not exhibit RV variations in available LAMOST spectra, but this could also be due to too few observations by LAMOST or false alarms by *Gaia* (RVs measured by *Gaia* are more reliable for cold stars).

However, high RUWE can also be caused by insufficient observation coverage, extreme crowding, background issues (such as nebulosity), magnitude perturbation, among others.

As noted in the *Gaia* documentation<sup>6</sup>, insufficient observation coverage can lead to spurious solutions, as a too small degree of freedom may have given a reasonable solution by chance only. To mitigate this effect, *Gaia* recommends requiring `visibility_periods_used > 11`. All 60 sources in our sample satisfy this criterion; therefore, their high RUWE values are unlikely to be caused by insufficient observational coverage.

The second and third factors may lead to a regional increase in RUWE. To examine whether the elevated RUWE values of these sources could be attributed to extreme crowding or background-related effects, we compare their RUWE values with those of neighboring sources within an angular distance of  $\leq 1$  arcmin. The neighboring sources are required to satisfy `visibility_periods_used > 11` and `astrometric_params_solved = 31` or `95` (corresponding to five-parameter and six-parameter astrometric solutions, respectively). We find that the RUWE values of most targets lie at the 100<sup>th</sup> percentile of the local RUWE distribution, i.e., most of them have the highest RUWE values among their neighbors. In

<sup>6</sup> <https://gea.esac.esa.int/archive/documentation/GDR3/index.html>

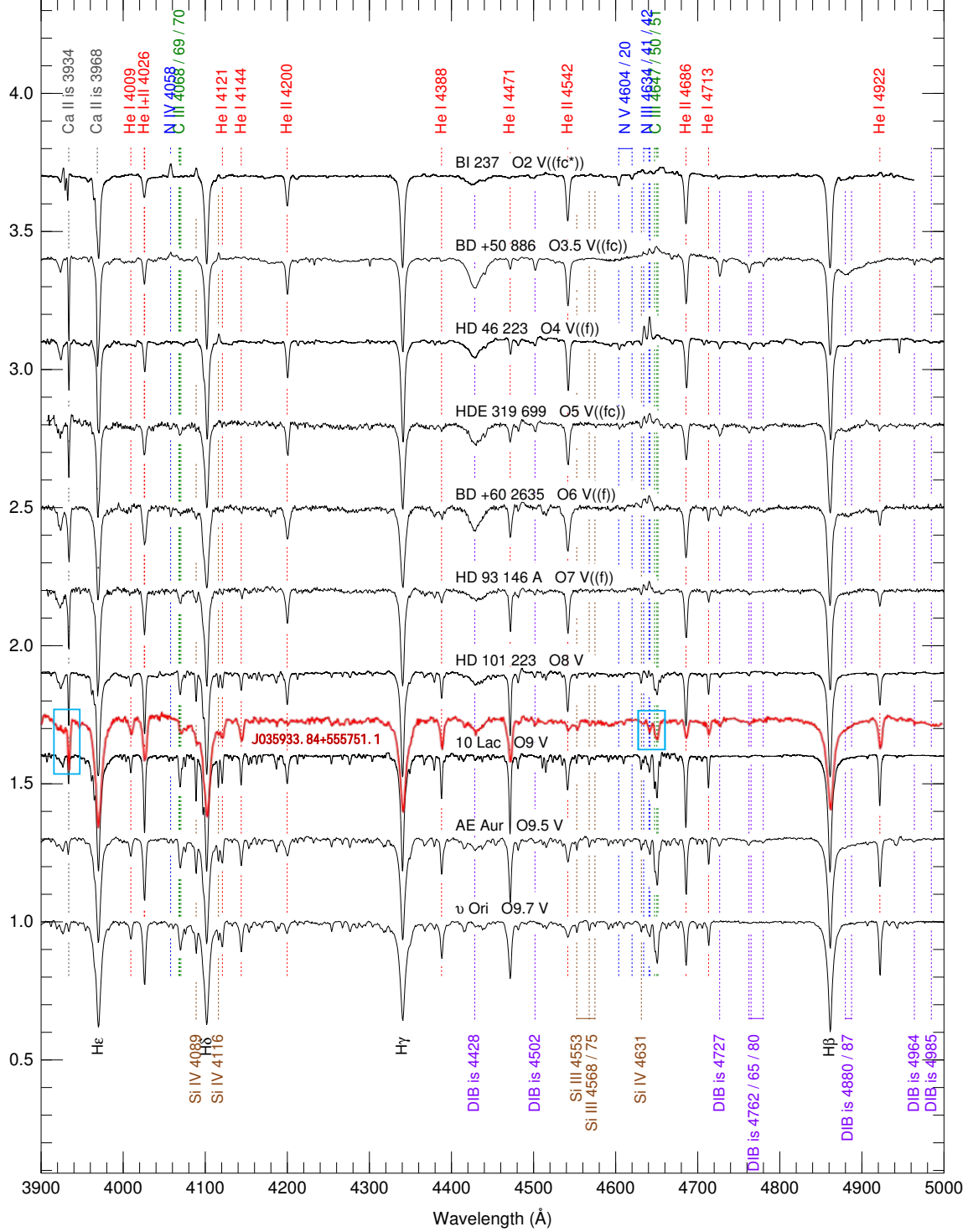


**Figure 5.** The contrast of spectral type sequence for O stars and LAMOST 035933.84+555751.1. The background figure is taken from J. Maíz Apellániz et al. (2026). The resolutions of spectra in background figure are  $\sim 2,500$ . The LAMOST/LRS spectrum (resolution:  $\sim 1,800$ ) of LAMOST 035933.84+555751.1 is plotted by red line and the key metal spectral lines to identify spectral type are highlighted by two blue squares.

addition, we quantify the local significance of the RUWE excess by defining a RUWE significance parameter:

$$\text{RUWE}_{\text{sig}} = \frac{\text{RUWE}_* - \text{median}(\text{RUWE}_{\text{neighbors}})}{1.4826 \times \text{MAD}(\text{RUWE}_{\text{neighbors}})}, \quad (3)$$

where  $\text{RUWE}_*$  is the RUWE value of the target source,  $\text{RUWE}_{\text{neighbors}}$  denotes the RUWE values of the neighboring sources, 'median' means taking the median and 'MAD' means taking the median absolute deviation. The factor 1.4826 rescales the RUWE significance parameter to be consistent with the standard deviation for a Gaussian distribution. The  $\text{RUWE}_{\text{sig}}$  values span the range 7.5 to 546.4, with a median of 28.9, indicating that these sources deviate by many robust standard deviations from the local RUWE distribution. This demonstrates that their elevated RUWE values are not mild statistical fluctuations but instead represent genuine local outliers. Generally, high RUWE values of these sources are unlikely to be caused by extreme crowding or background issues.

Magnitude perturbations can displace the centroid of the point-spread function and thus increase RUWE. For CBe stars, this effect may be enhanced by their large, variable circumstellar disks. Although these disks can extend to many stellar radii, the resulting photocenter excursions still remain much smaller than the spatial scale sampled by *Gaia*'s image-parameter-determination (IPD) process. In other words, the perturbations are extended relative to the stellar photosphere but remain effectively unresolved at the IPD level. Consequently, such magnitude perturbations generally do not generate multiple peaks in the IPD profile and therefore are not expected to produce high values of `ipd_frac_multi_peak`. By contrast, significantly elevated `ipd_frac_multi_peak` values most plausibly reflect genuine image blending, arising either from relatively wide companions at separations of several to tens of milliarcseconds, or coincidentally from unrelated close neighbors along the line of sight. Sources with high `ipd_frac_multi_peak` are thus plausible candidates for sources with distant companions, whereas for sources with low `ipd_frac_multi_peak` we cannot distinguish whether the elevated RUWE is caused by magnitude perturbations or by unresolved close companions.

In summary, high RUWE values of these sources are unlikely caused by insufficient observation coverage, extreme crowding or background issues. We recommend to preferably attend sources with high `ipd_frac_multi_peak` values when attempting to search for companions among these sources. These potential CBe star binaries are listed in Table 5.

**Table 5.** Potential CBe star binaries from LAMOST DR12

LAMOST designation	<i>Gaia</i> DR3 ID	N	visibility -periods_used	RUWE	Percentage <sup>1</sup> (%)	RUWE -sig	ipd_frac -multi_peak (%)	$\Delta RV^2$	New CBe star?
J040636.03+525022.5	275098088451178240	2	21	23.58	100.0	546.4	19		No
J054415.00+322732.6	3448185944950896384	2	17	20.80	100.0	439.6	57		Yes
J061434.56+225434.2	3425138463244391680	37	17	18.58	100.0	270.8	0		Yes
J053551.06+371645.7	189495713746035328	1	15	18.04	100.0	275.1	44		No
J051554.95+425532.8	207456785941426048	3	16	16.86	100.0	322.1	32		No
J055126.83+170829.6	3349946127197206016	1	16	16.59	100.0	220.9	2		No
J055336.52+401846.2	191595540436839296	4	17	14.35	100.0	256.3	46		No
J042105.03+502714.1	270720004945832064	4	19	12.84	100.0	166.8	0		No
J055052.59+354409.8	3455191517646066560	2	18	12.45	100.0	216.1	93		No
J061202.17+211717.5	3375360788715959552	45	15	10.80	100.0	147.5	0		No
J035933.84+555751.1	468716416747466752	12	22	10.32	100.0	156.7	56		Yes
J040151.09+545511.8	468403674405344256	3	23	9.91	100.0	188.1	0		No
J041750.14+532526.1	275370698611155584	4	21	9.68	100.0	222.4	0		No
J014620.23+611421.5	511217729481951616	1	27	9.49	98.9	158.6	0		No
J060806.15+130723.9	3344236736973246592	3	17	7.79	100.0	205.5	0		No
J035920.13+505620.1	250810048388652928	3	21	5.75	100.0	174.7	0		Yes
J054837.63+281710.2	3443128019662992128	5	17	5.51	100.0	46.8	28		No
J015645.74+635259.7	517984879952478592	1	30	5.34	100.0	128.2	0		No

**Table 5** continued on next page

**Table 5** (continued)

LAMOST designation	<i>Gaia</i> DR3 ID	N	visibility	RUWE	Percentage <sup>1</sup> (%)	RUWE	ipd_frac	$\Delta RV^2$	New CBe star?
		-periods_used				-sig	-multi_peak (%)		
J041238.36+463615.3	233962369156929920	4	17	5.17	100.0	84.5	20	123.19018	No
J070724.42+035254.9	3116370751776866560	3	15	4.88	100.0	40.3	0	198.60501	Yes
J050535.04+442648.4	205544627842417408	2	16	4.07	100.0	64.9	0		No
J040839.73+474244.5	246137776809763712	6	15	3.86	100.0	44.7	1		No
J064707.66+044232.0	3129237374282787584	10	16	3.79	100.0	60.1	3		No
J062108.40+044846.0	3317666596109523328	2	17	3.71	100.0	46.5	38		No
J044345.35+243908.8	147294464602944256	16	17	3.58	100.0	167.4	0		Yes
J025158.41+570147.2	460613256564267008	11	19	3.39	100.0	30.6	0		No
J204151.60+482727.9	2167790566919245568	1	29	2.90	100.0	41.2	0		No
J035622.12+484550.2	247082394733516032	6	21	2.89	100.0	52.5	48		No
J063752.74+083237.2	3326115827571757184	1	14	2.75	100.0	24.5	0		Yes
J065553.98+061214.4	3129869048013753344	2	14	2.52	100.0	25.9	0		No
J035101.91+493720.1	250284825427868800	5	20	2.38	100.0	24.0	45		No
J055546.16+305126.4	3444050814860576768	14	16	2.38	100.0	25.7	0		No
J063159.26-004955.7	3119142929834761600	1	16	2.34	100.0	16.1	38		Yes
J054154.33+360647.9	3455879949363891584	2	17	2.13	100.0	38.0	0		Yes
J035814.15+521024.2	251702194696320768	7	21	2.12	100.0	27.4	2		No
J034512.81+521437.7	443762965990465920	5	21	2.09	97.0	17.2	1		Yes
J040818.93+552455.0	276392351073731712	3	23	2.06	97.4	25.0	0		No
J043346.95+324528.0	172036564308761728	2	15	2.05	100.0	30.4	0		No
...	...	...	...	...	...	...	...	...	...

<sup>1</sup>: The percentile of CBe star's RUWE in the local RUWE distribution.

<sup>2</sup>: Maximum RV separation published by *Gaia* DR3 (km s<sup>-1</sup>).

**Notes.** The complete table is available in the online journal and at CDS.

## 5. SPATIAL DISTRIBUTION, CLUSTER MEMBERSHIP AND RUNAWAY STARS

The spatial distribution of these CBe stars in the Milky Way is shown in Figure 6. The same as Section 3.4, sources analyzed here and subsequent studies in this section are with relative distance uncertainty not exceeding 20%. These CBe stars are primarily distributed at low Galactic latitudes toward the Galactic Anti-Center — a spatial trend observed in both newly identified and previously known sources. This trend may be attributable to survey plan of LAMOST and the severe interstellar extinction toward the Galactic Center. In particular, we notice that two sources, LAMOST J193507.42+262713.5 and LAMOST J193559.39+285042.8, located at ( $X \sim 4.5$  kpc,  $Y \sim 7$  kpc), appear spatially isolated from the main concentration of the sample. They do not have widely used cross-identifications in SIMBAD and were previously reported only as part of survey-level samples (B. Shridharan et al. 2021) rather than being targets of dedicated studies. As discussed in Section 3.4, LAMOST J193507.42+262713.5 is classified as a B3 II star and lies above the main sequence in the HRD, with a De-reddened (BP - RP) = -0.26 and an absolute  $M_G = -3.69$ . LAMOST J193559.39+285042.8 is classified as a B3 IV star and lies on or near the main sequence in the HRD, with a De-reddened (BP - RP) = -0.30 and an absolute  $M_G = -1.64$ . Their locations in the HRD are broadly consistent with their spectroscopically derived luminosity classes and do not show any obvious contradictions, supporting the conclusion that estimates of their distances are (roughly) reliable. Their apparent isolation in the  $XY$  plane also reflects distance-dependent selection effects: at such a large distance only intrinsically bright stars remain detectable and classifiable.

We also attempt to identify potential cluster members in our samples. Clusters provide an advantageous context for astrophysical studies, as they consist of coeval stars with similar distances, ages, and chemical compositions. Confirmed membership would thus offer strong constraints on fundamental parameters of the CBe stars residing in such environments. We utilize the cluster catalog from E. L. Hunt & S. Reffert (2023), which was complied by the largest

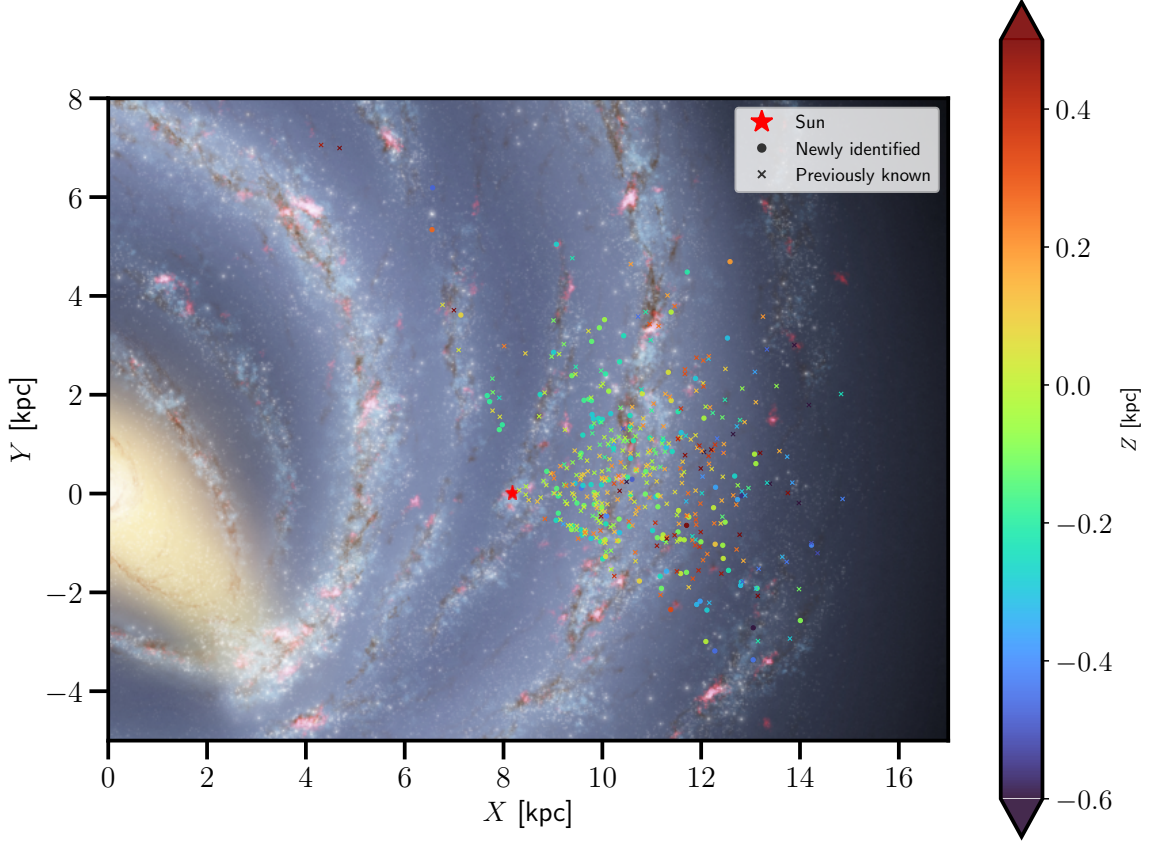


**Figure 6. Spatial distribution of CBe stars.** The background image comes from NASA/JPL-Caltech, created by R. Hurt (SSC/Caltech) and loaded by `mw_plot`. CBe stars newly identified by this work are marked by circles, while previously known CBe stars are marked by diagonal crosses. The heights of CBe stars above the Galactic plane are indicated by colors of respective marks. Additionally, we mark the Sun by a red pentagram.

blind search for star clusters to date based on *Gaia* data, containing 7,167 clusters. We cross-match our sample of CBe stars with this catalog and identify CBe stars as potential cluster members according to the following three criteria:

1. The angular separations between CBe stars and the densest points of clusters are less than total angular radii of corresponding clusters,
2. The distances to the CBe stars and clusters are consistent within  $1\sigma$ ,
3. The proper motions in both right ascension and declination between CBe stars and clusters are consistent within  $0.5 \text{ mas yr}^{-1}$ .

We identify 34 CBe stars as potential cluster members. Among these, seven are newly identified CBe stars in this work, and five are associated with two potential clusters each. These potential members and their host clusters are listed in Table 6.

Another interesting aspect of CBe stars is that how many are they runaway stars. Runaway stars are OB-type stars with large peculiar velocities, first identified by A. Blaauw & W. W. Morgan (1954). According to prevailing theories, such stars can be produced either by the supernova explosion of a binary companion (F. Zwicky 1957; A. Blaauw 1961) or through dynamical ejection from dense young clusters via gravitational interactions (A. Poveda et al. 1967). The study of runaway stars therefore provides valuable insights into the kinematics in supernova explosions and interactions between stars. To identify runaway stars within our sample, we calculate their peculiar velocities for sources with measured RVs. For a star in binary, this RV is actually the systemic velocity, which needs to be determined by solving the orbital parameters. For simplicity, we exclude RV-variable sources from calculating peculiar velocities. We also omit sources for which all available spectra had a SNR below 10. For the remaining objects, we use the spectrum with

highest SNR per source to measure its RV. Ultimately, a total of 203 sources with RV uncertainties below  $10 \text{ km s}^{-1}$  are retained for the peculiar velocity calculation.

To calculate peculiar velocities, we first calculate the 3D velocities in Galactocentric Cartesian frame ( $V_x$ ,  $V_y$  and  $V_z$ ) under the Milky way potential model `McMillan17` (P. J. McMillan 2017), the most used Milky way potential model by python package `galpy`<sup>7</sup> (J. Bovy 2015). The Sun is placed at  $(X, Z) = (-8.178, 0.025)$  kpc (J. Bland-Hawthorn & O. Gerhard 2016; `GRAVITY` Collaboration et al. 2019), with the circular velocity at the solar position of  $233.2 \text{ km s}^{-1}$  according to `McMillan17` at such place. The peculiar velocities of the Sun relative to the Local Standard of Rest is set to be  $(U_\odot, V_\odot, W_\odot) = (7.01, 10.13, 4.95) \text{ km s}^{-1}$  (Y. Huang et al. 2015). To determine the local rotational velocities of the Milky Way at given distance to the Galactic Center  $V_c$  for subsequent calculations, the  $V_x$ ,  $V_y$  and  $V_z$  we calculate are at the moment of Galactic plane crossing ( $Z = 0$ ), conducted by backward orbit integration in time of 1 Gyr.  $V_x$ ,  $V_y$  and  $V_z$  are then converted into 3D Galactic space velocity ( $U$ ,  $V$ ,  $W$ ) by the following matrix transformation:

$$\begin{bmatrix} -\cos \alpha & -\sin \alpha & 0 \\ -\sin \alpha & \cos \alpha & 0 \\ 0 & 0 & 1 \end{bmatrix} \begin{bmatrix} V_x \\ V_y \\ V_z \end{bmatrix} = \begin{bmatrix} U \\ V \\ W \end{bmatrix},$$

where  $\alpha$  is the angle between the Galactic Center-to-source vector and the positive X-axis in Galactocentric Cartesian frame. Ultimately, 3D peculiar velocities are derived as  $U_{\text{pec}} = U$ ,  $V_{\text{pec}} = V - V_c$ ,  $W_{\text{pec}} = W$  and  $V_{\text{pec,tot}} = \sqrt{U_{\text{pec}}^2 + V_{\text{pec}}^2 + W_{\text{pec}}^2}$ . Applying the classical criterion for runaway stars—a total peculiar velocity exceeding  $40 \text{ km s}^{-1}$  (e.g. A. Blaauw 1961; D. H. Berger & D. R. Gies 2001), we identify 37 runaway stars (13 newly identified CBe stars) with total peculiar velocities  $V_{\text{pec,tot}}$  ranging from  $\sim 40 \text{ km s}^{-1}$  to  $\sim 101 \text{ km s}^{-1}$ . In addition to `McMillan17`, we also calculate peculiar velocities utilizing other three Milky way potential models, including `MWPotential2014` (J. Bovy 2015), `Cautun20` (M. Cautun et al. 2020) and `Irrgang13I` (A. Irrgang et al. 2013), for reference. Peculiar velocities calculated by all the four models are listed in Table 7.

**Table 6.** Potential cluster members of CBe stars from LAMOST DR12.

LAMOST	<i>Gaia</i> DR3	pmra(s) <sup>1</sup>	pmdec(s) <sup>2</sup>	Dis.(s) <sup>3</sup>	New	Cluster	pmra(c) <sup>4</sup>	pmdec(c) <sup>5</sup>	Dis.(c) <sup>6</sup>
designation	ID	(mas yr <sup>-1</sup> )	(mas yr <sup>-1</sup> )	(kpc)	CBe star?	name	(mas yr <sup>-1</sup> )	(mas yr <sup>-1</sup> )	(kpc)
J000003.86+635429.6	431630851621447552	-1.97±0.01	-0.55±0.01	5.23 <sup>+0.33</sup> <sub>-0.35</sub>	No	HSC_937	-1.95±0.01	-0.52±0.01	4.82 <sup>+0.09</sup> <sub>-0.08</sub>
J011038.68+613922.2	522583690414836736	-1.82±0.01	-0.54±0.01	3.91 <sup>+0.21</sup> <sub>-0.18</sub>	Yes	UBC_1215	-1.77±0.01	-0.55±0.01	3.96±0.08
J011352.27+590144.6	414110030746911488	-0.99±0.01	-0.64±0.01	3.08 <sup>+0.14</sup> <sub>-0.11</sub>	No	NGC_436	-0.98±0.00	-0.66±0.00	3.19±0.02
J013357.02+615318.3	510782151078382208	-1.71±0.01	-0.41±0.01	3.07 <sup>+0.19</sup> <sub>-0.13</sub>	Yes	HSC_1025	-1.67±0.01	-0.25±0.01	2.92±0.06
J030427.62+561337.7	459627063352742912	0.97±0.02	-1.36±0.02	2.30 <sup>+0.08</sup> <sub>-0.07</sub>	Yes	UBC_1245	0.66±0.01	-1.03±0.01	2.35±0.03
J033851.13+515341.2	442195161187958272	0.70±0.01	-2.17±0.01	2.38 <sup>+0.08</sup> <sub>-0.07</sub>	No	UBC_1252	0.75±0.02	-2.13±0.02	2.43 <sup>+0.04</sup> <sub>-0.03</sub>
J035221.20+522835.7	251943984175934720	0.77±0.01	-1.53±0.01	2.18 <sup>+0.07</sup> <sub>-0.06</sub>	No	CWNU_1346	0.71±0.01	-2.00±0.01	2.25±0.03
						Teutsch_194	0.89±0.02	-1.53±0.02	2.13±0.03
J035612.84+581824.4	470023942230011520	-0.52±0.02	-0.05±0.01	4.26 <sup>+0.20</sup> <sub>-0.22</sub>	No	Juchert_9	-0.30±0.01	-0.11±0.01	4.43±0.11
J035712.14+555244.5	468740674721437568	-0.03±0.02	0.19±0.01	3.70 <sup>+0.27</sup> <sub>-0.21</sub>	No	HSC_1181	-0.01±0.00	-0.04±0.00	3.77±0.02
J044342.01+410424.7	203132441067857024	0.22±0.02	-1.36±0.02	3.01 <sup>+0.22</sup> <sub>-0.16</sub>	No	FSR_0723	0.00±0.03	-1.23±0.02	2.97±0.03
J052021.77+391925.9	187917223068585728	0.37±0.02	-1.38±0.01	2.77 <sup>+0.09</sup> <sub>-0.10</sub>	No	NGC_1857	0.47±0.00	-1.38±0.00	2.71±0.02
J052636.70+392052.4	193685540242156928	0.21±0.03	-0.63±0.02	4.36 <sup>+0.80</sup> <sub>-0.36</sub>	No	HSC_1322	0.10±0.01	-0.70±0.01	4.45 <sup>+0.10</sup> <sub>-0.09</sub>
J052701.81+423622.7	195434554004220032	-0.05±0.02	-0.37±0.02	4.23 <sup>+0.28</sup> <sub>-0.29</sub>	No	HSC_1300	0.10±0.02	-0.29±0.01	4.09±0.08
J052935.27+361306.0	183375007391969408	-0.18±0.03	-1.98±0.02	1.89±0.06	No	UBC_198	-0.01±0.01	-1.99±0.01	1.83±0.01
J054153.93+323613.1	3448388529968087040	-0.12±0.03	-0.78±0.02	3.44 <sup>+0.53</sup> <sub>-0.36</sub>	No	HSC_1381	-0.10±0.01	-0.78±0.02	3.65±0.08

**Table 6** continued on next page

<sup>7</sup> <http://github.com/jobovy/galpy>

**Table 6** (continued)

LAMOST	<i>Gaia</i> DR3	pmra(s) <sup>1</sup>	pmdec(s) <sup>2</sup>	Dis.(s) <sup>3</sup>	New	Cluster	pmra(c) <sup>4</sup>	pmdec(c) <sup>5</sup>	Dis.(c) <sup>6</sup>
designation	ID	(mas yr <sup>-1</sup> )	(mas yr <sup>-1</sup> )	(kpc)	CBe star?	name	(mas yr <sup>-1</sup> )	(mas yr <sup>-1</sup> )	(kpc)
J055304.96+252606.6	3428324809286029056	0.36±0.03	-1.67±0.02	2.48 <sup>+0.16</sup> <sub>-0.14</sub>	No	UBC_1299	0.55±0.01	-1.47±0.01	2.59 <sup>+0.04</sup> <sub>-0.03</sub>
J060017.47+234019.4	3424861897411791744	0.27±0.02	-2.15±0.01	1.82±0.05	No	NGC_2129	0.22±0.01	-2.19±0.01	1.86±0.01
J060452.44+240331.3	3426200454038524928	0.93±0.02	-3.07±0.02	1.94±0.07	No	IC_2157	0.98±0.01	-3.02±0.01	1.94±0.01
J061007.35+244201.1	3426316418155789696	0.23±0.02	-0.45±0.01	3.73 <sup>+0.20</sup> <sub>-0.21</sub>	No	FSR_0869	0.51±0.01	-0.44±0.01	3.91 <sup>+0.10</sup> <sub>-0.09</sub>
J061250.77+093035.0	3329082168206416000	-0.42±0.02	-1.01±0.02	2.32 <sup>+0.09</sup> <sub>-0.10</sub>	Yes	HSC_1585	-0.37±0.01	-1.14±0.02	2.41±0.03
J061931.75+140346.8	3344634107345773568	0.24±0.02	-2.11±0.02	3.21 <sup>+0.14</sup> <sub>-0.16</sub>	Yes	UBC_1316	0.53±0.01	-1.83±0.02	3.09±0.05
J062104.61+221010.1	3376778299723392512	0.22±0.02	-2.36±0.02	1.74 <sup>+0.04</sup> <sub>-0.05</sub>	No	OC_0315	0.62±0.02	-2.50±0.02	1.69±0.01
						OC_0316	0.25±0.01	-2.35±0.01	1.71±0.02
J062806.24+174537.3	3369789906895933824	0.26±0.02	-0.74±0.01	3.77 <sup>+0.13</sup> <sub>-0.15</sub>	No	HSC_1540	-0.07±0.01	-0.41±0.02	3.90 <sup>+0.07</sup> <sub>-0.06</sub>
J062915.48+171630.7	3369689610820311552	-0.15±0.02	-0.21±0.02	3.61 <sup>+0.27</sup> <sub>-0.21</sub>	Yes	HSC_1540	-0.07±0.01	-0.41±0.02	3.90 <sup>+0.07</sup> <sub>-0.06</sub>
J063500.45+171044.7	3358945453772420224	-0.17±0.02	-0.21±0.01	3.86 <sup>+0.23</sup> <sub>-0.20</sub>	No	HSC_1552	0.00±0.02	-0.51±0.02	3.79±0.07
J063653.75+133219.2	3355441688172411648	-0.03±0.02	-0.17±0.02	4.09 <sup>+0.16</sup> <sub>-0.18</sub>	No	HSC_1583	0.04±0.01	-0.33±0.02	4.18 <sup>+0.08</sup> <sub>-0.07</sub>
J063701.44+051307.1	3130981135303925120	-1.49±0.02	0.80±0.02	1.46±0.04	No	Collinder_104	-1.39±0.01	0.65±0.01	1.51±0.01
						HSC_1629	-1.21±0.02	0.58±0.02	1.43±0.01
J063703.39+171837.0	3358961465412197888	-0.37±0.02	-0.30±0.02	3.95 <sup>+0.33</sup> <sub>-0.28</sub>	No	HSC_1552	0.00±0.02	-0.51±0.02	3.79±0.07
J063809.24+034454.6	3130207762014534144	-2.32±0.02	-0.28±0.01	1.38±0.03	Yes	Collinder_107	-2.43±0.01	-0.20±0.02	1.41±0.01
J063854.52+003418.5	3119809650489626880	-0.35±0.03	0.61±0.02	5.81 <sup>+0.56</sup> <sub>-0.49</sub>	No	HSC_1665	-0.21±0.01	0.39±0.01	5.71±0.14
J065025.97+113923.4	3351354734735237376	0.07±0.02	-0.40±0.02	4.09 <sup>+0.37</sup> <sub>-0.27</sub>	No	Juchert_J0649.4+1202	0.04±0.01	-0.39±0.01	4.03±0.07
J202010.60+383732.1	2061287708824637440	-3.57±0.01	-5.73±0.02	1.73±0.04	No	Berkeley_86	-3.45±0.01	-5.47±0.01	1.68±0.01
						FoF_2179	-3.25±0.01	-5.99±0.01	1.70±0.01
J213057.76+525020.6	2172650099079727488	-2.52±0.02	-2.77±0.02	2.85±0.13	No	Theia_5761	-2.91±0.01	-3.13±0.01	2.99±0.03
J230456.23+573851.2	2010162896331826944	-3.54±0.01	-2.42±0.01	3.20 <sup>+0.15</sup> <sub>-0.10</sub>	No	Casado_19	-3.28±0.01	-2.30±0.01	3.33±0.03

<sup>1</sup>: Proper motion in right ascension direction of the CBe star.<sup>2</sup>: Proper motion in declination direction of the CBe star.<sup>3</sup>: Distance of the CBe star.<sup>4</sup>: Proper motion in right ascension direction of the cluster.<sup>5</sup>: Proper motion in declination direction of the cluster.<sup>6</sup>: Distance of the cluster.**Table 7.** Peculiar velocities of partial CBe stars from LAMOST DR12.

<i>Gaia</i> DR3	RV	pmra(s)	pmdec(s)	Dis.(s)	New	N	$V_{\text{pec,McMillan17}}$	$V_{\text{pec,MWPotential2014}}$	$V_{\text{pec,Cautun20}}$	$V_{\text{pec,Irrgang13I}}$
ID	(km s <sup>-1</sup> )	(mas yr <sup>-1</sup> )	(mas yr <sup>-1</sup> )	(kpc)	CBe star?	(km s <sup>-1</sup> )	(km s <sup>-1</sup> )	(km s <sup>-1</sup> )	(km s <sup>-1</sup> )	(km s <sup>-1</sup> )
943635960251342592	-42.99 <sup>+4.32</sup> <sub>-4.41</sub>	3.01±0.02	-5.69±0.02	2.25 <sup>+0.11</sup> <sub>-0.10</sub>	No	2	100.68	97.42	86.19	81.53
2104951725038702336	-64.86 <sup>+5.74</sup> <sub>-5.62</sub>	-4.49±0.03	-10.17±0.03	4.08 <sup>+0.53</sup> <sub>-0.48</sub>	No	6	99.69	106.05	112.61	138.61
202496328496716256	49.91 <sup>+5.97</sup> <sub>-5.94</sub>	-2.41±0.01	-6.02±0.01	8.06 <sup>+0.80</sup> <sub>-0.64</sub>	No	1	87.74	100.79	66.38	97.62
3119809650489626880	-33.57 <sup>+5.60</sup> <sub>-5.29</sub>	-0.35±0.03	0.61±0.02	5.81 <sup>+0.56</sup> <sub>-0.49</sub>	No	1	78.87	95.32	84.09	100.91
511217488963795584	-112.65 <sup>+9.29</sup> <sub>-9.81</sub>	-1.07±0.01	-0.23±0.01	2.88 <sup>+0.10</sup> <sub>-0.11</sub>	No	1	72.03	67.09	77.81	90.27
2013258876254822016	61.45 <sup>+6.74</sup> <sub>-6.57</sub>	-2.91±0.02	-2.11±0.02	1.66 <sup>+0.07</sup> <sub>-0.06</sub>	No	1	70.75	105.73	96.77	71.80
3153828952571014528	87.84 <sup>+9.06</sup> <sub>-8.94</sub>	-0.63±0.02	-1.52±0.02	1.68±0.07	No	4	70.17	47.87	49.04	63.85
511257140102787584	-109.95 <sup>+4.25</sup> <sub>-4.23</sub>	-1.50±0.01	-0.19±0.01	3.44 <sup>+0.25</sup> <sub>-0.22</sub>	Yes	2	67.36	68.10	49.81	70.44
1871130372560308992	2.44 <sup>+4.41</sup> <sub>-4.74</sub>	4.15±0.01	-1.21±0.01	2.09 <sup>+0.06</sup> <sub>-0.05</sub>	No	2	67.00	55.88	74.77	78.33

**Table 7** continued on next page

**Table 7** (continued)

<i>Gaia</i> DR3	RV	pmra(s)	pmdec(s)	Dis.(s)	New	N	$V_{\text{pec,McMillan17}}$	$V_{\text{pec,MWPotential2014}}$	$V_{\text{pec,Cautun20}}$	$V_{\text{pec,Irrgang13I}}$
ID	(km s <sup>-1</sup> )	(mas yr <sup>-1</sup> )	(mas yr <sup>-1</sup> )	(kpc)	CBe star?		(km s <sup>-1</sup> )	(km s <sup>-1</sup> )	(km s <sup>-1</sup> )	(km s <sup>-1</sup> )
273756340665255424	-71.63 <sup>+5.34</sup> <sub>-5.61</sub>	2.36 $\pm$ 0.02	-3.85 $\pm$ 0.01	0.88 $\pm$ 0.01	No	6	65.03	75.62	72.53	73.94
442195161187958272	-87.25 <sup>+8.11</sup> <sub>-8.65</sub>	0.70 $\pm$ 0.01	-2.17 $\pm$ 0.01	2.38 <sup>+0.08</sup> <sub>-0.07</sub>	No	20	63.35	81.51	55.67	80.35
459871498533427328	-71.77 <sup>+9.58</sup> <sub>-9.98</sub>	0.52 $\pm$ 0.01	-1.38 $\pm$ 0.02	2.10 <sup>+0.06</sup> <sub>-0.07</sub>	Yes	6	63.00	57.38	51.33	50.10
2006919818073117952	-76.13 <sup>+8.46</sup> <sub>-8.55</sub>	-2.63 $\pm$ 0.02	-3.57 $\pm$ 0.02	2.08 <sup>+0.07</sup> <sub>-0.06</sub>	Yes	2	62.57	46.14	52.92	64.31
37694252194590976	-33.68 <sup>+7.04</sup> <sub>-7.29</sub>	-2.02 $\pm$ 0.04	-1.65 $\pm$ 0.03	2.76 <sup>+0.29</sup> <sub>-0.24</sub>	No	5	61.60	71.78	71.87	73.60
2003956939163275136	-85.35 <sup>+3.99</sup> <sub>-4.14</sub>	-3.38 $\pm$ 0.01	-2.82 $\pm$ 0.01	2.98 <sup>+0.09</sup> <sub>-0.10</sub>	Yes	2	59.65	44.54	58.24	54.98
1864444345433406592	-82.45 <sup>+3.40</sup> <sub>-3.29</sub>	-3.93 $\pm$ 0.01	-5.60 $\pm$ 0.01	6.41 <sup>+0.31</sup> <sub>-0.38</sub>	Yes	1	56.74	73.75	55.77	52.32
241341226047485312	18.05 <sup>+1.69</sup> <sub>-1.65</sub>	1.94 $\pm$ 0.03	-3.54 $\pm$ 0.03	2.65 <sup>+0.19</sup> <sub>-0.16</sub>	No	3	51.74	47.97	64.27	56.57
270346377148562816	-99.84 <sup>+9.41</sup> <sub>-9.44</sub>	0.26 $\pm$ 0.02	-0.71 $\pm$ 0.02	3.74 <sup>+0.30</sup> <sub>-0.27</sub>	Yes	1	51.67	76.04	48.87	75.07
183440737570824448	-54.18 <sup>+6.54</sup> <sub>-6.77</sub>	0.80 $\pm$ 0.02	-1.72 $\pm$ 0.02	2.81 <sup>+0.16</sup> <sub>-0.12</sub>	No	16	51.67	37.81	54.77	45.92
3088286686477378304	-43.06 <sup>+8.13</sup> <sub>-8.57</sub>	-1.51 $\pm$ 0.06	-0.82 $\pm$ 0.04	0.87 <sup>+0.04</sup> <sub>-0.03</sub>	No	4	49.73	64.99	54.61	60.59
3374580582137345408	-46.61 <sup>+6.21</sup> <sub>-6.25</sub>	0.55 $\pm$ 0.03	-3.86 $\pm$ 0.02	1.47 $\pm$ 0.06	No	1	49.66	40.62	54.12	51.78
3326790721553428736	-43.26 <sup>+6.05</sup> <sub>-6.16</sub>	-1.85 $\pm$ 0.02	-2.81 $\pm$ 0.02	1.01 <sup>+0.02</sup> <sub>-0.03</sub>	Yes	4	49.49	64.59	56.96	54.12
448859820863017472	-93.34 <sup>+8.27</sup> <sub>-8.10</sub>	0.51 $\pm$ 0.02	-0.03 $\pm$ 0.02	4.86 <sup>+0.40</sup> <sub>-0.42</sub>	No	2	49.20	39.13	61.91	48.59
2016382386934503168	-74.41 <sup>+5.93</sup> <sub>-5.88</sub>	-5.27 $\pm$ 0.01	-0.46 $\pm$ 0.01	2.67 <sup>+0.09</sup> <sub>-0.07</sub>	Yes	1	49.04	48.66	48.10	45.97
3425142311534938112	-48.08 <sup>+6.21</sup> <sub>-6.50</sub>	0.00 $\pm$ 0.02	-0.87 $\pm$ 0.02	4.14 <sup>+0.28</sup> <sub>-0.25</sub>	No	64	48.09	48.81	50.23	69.16
189638096203389440	-57.93 <sup>+6.70</sup> <sub>-6.85</sub>	-0.41 $\pm$ 0.02	-1.53 $\pm$ 0.01	3.45 <sup>+0.17</sup> <sub>-0.16</sub>	No	1	48.00	55.25	55.90	47.13
184522519573582848	-66.85 <sup>+6.19</sup> <sub>-6.43</sub>	0.40 $\pm$ 0.02	-1.38 $\pm$ 0.01	2.74 <sup>+0.14</sup> <sub>-0.13</sub>	Yes	1	47.81	63.04	63.82	45.79
247190868429680384	31.93 <sup>+6.85</sup> <sub>-6.95</sub>	0.74 $\pm$ 0.01	-1.93 $\pm$ 0.01	2.18 <sup>+0.09</sup> <sub>-0.05</sub>	No	1	45.94	50.25	38.55	51.08
3369789906895933824	-16.13 <sup>+7.49</sup> <sub>-7.26</sub>	0.26 $\pm$ 0.02	-0.74 $\pm$ 0.01	3.77 <sup>+0.13</sup> <sub>-0.15</sub>	No	18	44.17	44.77	33.98	46.88
3107967257426335104	105.29 <sup>+7.86</sup> <sub>-7.55</sub>	-1.79 $\pm$ 0.02	0.45 $\pm$ 0.02	4.94 <sup>+0.82</sup> <sub>-0.77</sub>	Yes	1	44.09	45.29	44.32	40.86
458436120468296960	-67.36 <sup>+3.31</sup> <sub>-3.35</sub>	-0.49 $\pm$ 0.02	-1.04 $\pm$ 0.02	2.28 <sup>+0.11</sup> <sub>-0.12</sub>	Yes	1	43.11	47.49	43.04	36.71
3127578146818103040	69.44 <sup>+3.17</sup> <sub>-3.19</sub>	-1.07 $\pm$ 0.03	-0.40 $\pm$ 0.02	2.04 $\pm$ 0.09	Yes	6	42.05	40.55	40.80	35.26
3120658331728894080	46.23 <sup>+1.69</sup> <sub>-1.75</sub>	-0.02 $\pm$ 0.02	-2.21 $\pm$ 0.02	2.31 $\pm$ 0.09	No	4	41.91	38.34	43.11	36.09
2007475277604631040	-54.98 $\pm$ 7.07	-1.74 $\pm$ 0.02	-2.37 $\pm$ 0.02	2.14 $\pm$ 0.06	No	2	41.74	29.29	42.80	38.09
245140004363839488	-60.31 <sup>+5.23</sup> <sub>-5.15</sub>	0.91 $\pm$ 0.02	-2.16 $\pm$ 0.01	1.57 <sup>+0.06</sup> <sub>-0.05</sub>	No	4	41.67	51.96	51.17	52.77
512033086070875136	-68.39 <sup>+6.55</sup> <sub>-6.73</sub>	-1.26 $\pm$ 0.01	-0.28 $\pm$ 0.01	2.46 $\pm$ 0.06	Yes	3	41.66	29.97	42.65	40.37
3455386161265334400	-34.80 <sup>+8.78</sup> <sub>-9.13</sub>	0.52 $\pm$ 0.02	-3.31 $\pm$ 0.01	2.24 $\pm$ 0.07	No	2	40.33	42.92	36.04	39.46
...	...	...	...	...	...	...	...	...	...	...

**Notes.** The complete table is available in the online journal and at CDS.

## 6. SUMMARY AND DISCUSSION

CBe stars are rapidly rotating B-type stars whose high rotational speeds promote the formation of decretion disks—composed of material ejected from the stellar equator—that give rise to characteristic H $\alpha$  emission. Given that the majority of CBe stars are thought to form through binary interactions, identifying and characterizing these systems presents a valuable opportunity to study binary evolution processes. To this end, we conduct a systematic search for CBe stars and CBe star binaries using data from LAMOST. Our main results are as follows:

1. *CBe stars:* We construct the initial O/B star sample by utilizing `subclass` of LAMOST DR12. Among them, we identify 504 CBe stars including 141 newly identified by inspecting their spectra by eye-checking with two criteria applied, cross-matching with CBe star catalogs and IR test.
2. *CBe star binaries:* 14 CBe stars exhibit significant RV variability with maximum RV separations ranging from  $\sim$ 20 km s $^{-1}$  to  $\sim$ 130 km s $^{-1}$ . One of them, ALS 8814, has previously been reported as CBe star binaries, while another two have been identified as (First Degree Trend) SB1 by *Gaia* DR3. For other 11 newly identified CBe star binaries, we briefly discuss LAMOST J035933.84+555751.1.

3. *Potential CBe star binaries*: We also propose 60 CBe stars as potential CBe star binaries which is with high RUWE but not confirmed by dynamics.
4. *Potential cluster members*: By comparing distances, angular separations and proper motions between sources in our samples and clusters, we find 34 CBe stars are potential cluster members.
5. *Runaway stars*: We calculate peculiar velocities for 203 CBe stars and identify 37 runaway stars adopting the classical criterion for runaway stars (total peculiar velocity exceeding  $40 \text{ km s}^{-1}$ ).

Of the CBe stars in our sample, only  $\sim 3\%$  exhibit RV variability. This rate is undoubtedly sensitive to the number of observations of the sample to a certain extent. When considering only sources with at least five observations, the detection rate rises to 7.9%. For comparison, L. Wang et al. (2018) performed a systematic search for Be+sdO binaries using far-ultraviolet (FUV) spectra from the International Ultraviolet Explorer (*IUE*), reporting a detection rate of  $\sim 4.5\%$  —somewhat lower than our detection rate. More recently, V. M. Kalari et al. (2025) presented speckle observations of 76 Be stars taken using the Gemini North and South speckle imagers spanning angular separations of 20 mas–1.2'' and reported an observed binary detection rate of 14.5%, the highest among the three studies.

Given that RV monitoring is less sensitive to widely separated and/or low-inclination systems, and considering that the spanning angular separations in V. M. Kalari et al. (2025) remain below the spatial resolution of *IUE*, the comparatively higher detection rates in this study and V. M. Kalari et al. (2025) may suggest that companions with faint FUV radiations (compared to the primary CBe stars), such as compact objects or puffed-up helium stars, are more common than sdOs as companions to CBe stars. This inference is consistent with the theoretical predictions of Y. Shao & X.-D. Li (2014). But overall, each of the three methods has their own advantages and disadvantages and all three yield detection rates of the same order of magnitude, underscoring their complementary roles in identifying CBe star binaries.

We report a runaway rate of 18.2% for CBe stars in our sample, which is significantly higher than the rates of  $\sim 6.7\%$  and  $\sim 5\%$  reported by D. H. Berger & D. R. Gies (2001) and L. Wang et al. (2022), respectively, both of which adopted the same threshold as us. We acknowledge that due to the scarcity and/or concentration of corresponding phases of the available spectra, some CBe stars discussed here may be RV-variable but are mistaken for RV-constant, despite our filtering of objects with observed RV variations. There is no doubt that restricting our analysis to sources with multiple observations can significantly reduce potential binarity contamination. The runaway rates are 10.9% ( $\geq 3$  observations), 12.1% ( $\geq 4$  observations), 10.6% ( $\geq 5$  observations) and 11.0% ( $\geq 6$  observations), respectively. Therefore, the true runaway rate in our sample is likely not less than 10%. The lower rate found by D. H. Berger & D. R. Gies (2001) may be influenced by their sample selection, which included only stars brighter than  $V = 9$  and thus primarily probed the solar neighborhood. L. Wang et al. (2022) suggested that the absence of RV measurements in their study likely resulted in incomplete detection of runaway stars. Furthermore, Y. Guo et al. (2024) reported a runaway rate of  $\sim 5\%$  among 4,432 early-type stars with measured RVs, a value much lower than our derived rate for CBe stars. If there are indeed differences between the runaway rates of early type stars and CBe stars, it may be another evidence that CBe stars prefer to form through binary interactions, as a systematically higher runaway fraction of CBe stars would suggest that CBe stars are more likely to form in evolved systems that have experienced supernova explodes compared to the general population of early-type stars.

#### ACKNOWLEDGMENTS

We thank Luqian Wang for helpful discussions. We acknowledge the Milky Way face-on background image provided by NASA/JPL-Caltech, created by R. Hurt (SSC/Caltech). This work was supported by the National Key R&D Program of China under grants 2021YFA1600401 and 2023YFA1607901, the National Natural Science Foundation of China under grants 12433007 and 12221003. We acknowledge the science research grants from the China Manned Space Project with No. CMS-CSST-2025-A13. This paper uses the data from the LAMOST survey. Guoshoujing Telescope (the Large Sky Area Multi-Object Fiber Spectroscopic Telescope LAMOST) is a National Major Scientific Project built by the Chinese Academy of Sciences. Funding for the project has been provided by the National Development and Reform Commission. LAMOST is operated and managed by the National Astronomical Observatories, Chinese Academy of Sciences. This work has made use of data from the European Space Agency (ESA) mission Gaia (<https://www.cosmos.esa.int/gaia>), processed by the Gaia Data Processing and Analysis Consortium (DPAC,

<https://www.cosmos.esa.int/web/gaia/dpac/consortium>). Funding for the DPAC has been provided by national institutions, in particular the institutions participating in the Gaia Multilateral Agreement. This research has made use of the SIMBAD database, CDS, Strasbourg Astronomical Observatory, France. This research has made use of the VizieR catalogue access tool, CDS, Strasbourg, France (F. Ochsenbein 1996). The original description of the VizieR service was published in F. Ochsenbein et al. (2000).

*Facilities:* LAMOST, *Gaia*

*Software:* Astropy (Astropy Collaboration et al. 2013, 2018, 2022), Numpy (C. R. Harris et al. 2020), Pandas (T. pandas development team 2020), laspec (B. Zhang et al. 2020, 2021), matplotlib (J. D. Hunter 2007), emcee (D. Foreman-Mackey et al. 2013), mw\_plot ([milkyway\\_plot](#)), Vizier (F. Ochsenbein et al. 2000), Simbad (M. Wenger et al. 2000), galpy (J. Bovy 2015)

## REFERENCES

Abt, H. A. 1979, ApJ, 230, 485, doi: [10.1086/157104](https://doi.org/10.1086/157104)

Amôres, E. B., Jesus, R. M., Moitinho, A., et al. 2021, MNRAS, 508, 1788, doi: [10.1093/mnras/stab2248](https://doi.org/10.1093/mnras/stab2248)

An, Q.-Y., Huang, Y., Gu, W.-M., et al. 2025, arXiv e-prints, arXiv:2505.23151, doi: [10.48550/arXiv.2505.23151](https://doi.org/10.48550/arXiv.2505.23151)

Astropy Collaboration, Robitaille, T. P., Tollerud, E. J., et al. 2013, A&A, 558, A33, doi: [10.1051/0004-6361/201322068](https://doi.org/10.1051/0004-6361/201322068)

Astropy Collaboration, Price-Whelan, A. M., Sipócz, B. M., et al. 2018, AJ, 156, 123, doi: [10.3847/1538-3881/aabc4f](https://doi.org/10.3847/1538-3881/aabc4f)

Astropy Collaboration, Price-Whelan, A. M., Lim, P. L., et al. 2022, ApJ, 935, 167, doi: [10.3847/1538-4357/ac7c74](https://doi.org/10.3847/1538-4357/ac7c74)

Bailer-Jones, C. A. L., Rybizki, J., Fouesneau, M., Demleitner, M., & Andrae, R. 2021, AJ, 161, 147, doi: [10.3847/1538-3881/abd806](https://doi.org/10.3847/1538-3881/abd806)

Banyard, G., Sana, H., Mahy, L., et al. 2022, A&A, 658, A69, doi: [10.1051/0004-6361/202141037](https://doi.org/10.1051/0004-6361/202141037)

Bayo, A., Rodrigo, C., Barrado Y Navascués, D., et al. 2008, A&A, 492, 277, doi: [10.1051/0004-6361:200810395](https://doi.org/10.1051/0004-6361:200810395)

Berger, D. H., & Gies, D. R. 2001, ApJ, 555, 364, doi: [10.1086/321461](https://doi.org/10.1086/321461)

Blaauw, A. 1961, BAN, 15, 265

Blaauw, A., & Morgan, W. W. 1954, ApJ, 119, 625, doi: [10.1086/145866](https://doi.org/10.1086/145866)

Bland-Hawthorn, J., & Gerhard, O. 2016, ARA&A, 54, 529, doi: [10.1146/annurev-astro-081915-023441](https://doi.org/10.1146/annurev-astro-081915-023441)

Bodenheimer, P. 1995, ARA&A, 33, 199, doi: [10.1146/annurev.aa.33.090195.001215](https://doi.org/10.1146/annurev.aa.33.090195.001215)

Bodensteiner, J., Sana, H., Wang, C., et al. 2021, A&A, 652, A70, doi: [10.1051/0004-6361/202140507](https://doi.org/10.1051/0004-6361/202140507)

Bovy, J. 2015, ApJS, 216, 29, doi: [10.1088/0067-0049/216/2/29](https://doi.org/10.1088/0067-0049/216/2/29)

Cardelli, J. A., Clayton, G. C., & Mathis, J. S. 1989, ApJ, 345, 245, doi: [10.1086/167900](https://doi.org/10.1086/167900)

Cautun, M., Benítez-Llambay, A., Deason, A. J., et al. 2020, MNRAS, 494, 4291, doi: [10.1093/mnras/staa1017](https://doi.org/10.1093/mnras/staa1017)

Chen, P. S., Liu, J. Y., & Shan, H. G. 2016, MNRAS, 463, 1162, doi: [10.1093/mnras/stw1757](https://doi.org/10.1093/mnras/stw1757)

Chojnowski, S. D., Whelan, D. G., Wisniewski, J. P., et al. 2015, AJ, 149, 7, doi: [10.1088/0004-6256/149/1/7](https://doi.org/10.1088/0004-6256/149/1/7)

Cui, X.-Q., Zhao, Y.-H., Chu, Y.-Q., et al. 2012, Research in Astronomy and Astrophysics, 12, 1197, doi: [10.1088/1674-4527/12/9/003](https://doi.org/10.1088/1674-4527/12/9/003)

Cutri, R. M., Skrutskie, M. F., van Dyk, S., et al. 2003, VizieR Online Data Catalog: 2MASS All-Sky Catalog of Point Sources (Cutri+ 2003),, VizieR On-line Data Catalog: II/246. Originally published in: University of Massachusetts and Infrared Processing and Analysis Center, (IPAC/California Institute of Technology) (2003)

Cutri, R. M., Wright, E. L., Conrow, T., et al. 2021, VizieR Online Data Catalog: AllWISE Data Release (Cutri+ 2013),, VizieR On-line Data Catalog: II/328. Originally published in: IPAC/Caltech (2013)

Du, B., Luo, A. L., Zhang, S., et al. 2021, Research in Astronomy and Astrophysics, 21, 202, doi: [10.1088/1674-4527/21/8/202](https://doi.org/10.1088/1674-4527/21/8/202)

Dunstall, P. R., Brott, I., Dufton, P. L., et al. 2011, A&A, 536, A65, doi: [10.1051/0004-6361/201117588](https://doi.org/10.1051/0004-6361/201117588)

Ekström, S., Meynet, G., Maeder, A., & Barblan, F. 2008, A&A, 478, 467, doi: [10.1051/0004-6361:20078095](https://doi.org/10.1051/0004-6361:20078095)

El-Badry, K., Fabry, M., Sana, H., Shenar, T., & Seeburgen, R. 2025, The Open Journal of Astrophysics, 8, 128, doi: [10.33232/001c.143907](https://doi.org/10.33232/001c.143907)

Finkenzeller, U., & Mundt, R. 1984, A&AS, 55, 109

Foreman-Mackey, D., Hogg, D. W., Lang, D., & Goodman, J. 2013, PASP, 125, 306, doi: [10.1086/670067](https://doi.org/10.1086/670067)

Gaia Collaboration, Vallenari, A., Brown, A. G. A., et al. 2023, A&A, 674, A1, doi: [10.1051/0004-6361/202243940](https://doi.org/10.1051/0004-6361/202243940)

Gaia Collaboration, Panuzzo, P., Mazeh, T., et al. 2024, A&A, 686, L2, doi: [10.1051/0004-6361/202449763](https://doi.org/10.1051/0004-6361/202449763)

Granada, A., Ekström, S., Georgy, C., et al. 2013, A&A, 553, A25, doi: [10.1051/0004-6361/201220559](https://doi.org/10.1051/0004-6361/201220559)

GRAVITY Collaboration, Abuter, R., Amorim, A., et al. 2019, *A&A*, 625, L10, doi: [10.1051/0004-6361/201935656](https://doi.org/10.1051/0004-6361/201935656)

Green, G. M., Schlaflay, E., Zucker, C., Speagle, J. S., & Finkbeiner, D. 2019, *ApJ*, 887, 93, doi: [10.3847/1538-4357/ab5362](https://doi.org/10.3847/1538-4357/ab5362)

Guo, Y., Wang, L., Liu, C., et al. 2024, *ApJS*, 272, 45, doi: [10.3847/1538-4365/ad46f8](https://doi.org/10.3847/1538-4365/ad46f8)

Harris, C. R., Millman, K. J., van der Walt, S. J., et al. 2020, *Nature*, 585, 357, doi: [10.1038/s41586-020-2649-2](https://doi.org/10.1038/s41586-020-2649-2)

Hastings, B., Wang, C., & Langer, N. 2020, *A&A*, 633, A165, doi: [10.1051/0004-6361/201937018](https://doi.org/10.1051/0004-6361/201937018)

Hou, W., Luo, A. L., Hu, J.-Y., et al. 2016, *Research in Astronomy and Astrophysics*, 16, 138, doi: [10.1088/1674-4527/16/9/138](https://doi.org/10.1088/1674-4527/16/9/138)

Huang, W., Gies, D. R., & McSwain, M. V. 2010, *ApJ*, 722, 605, doi: [10.1088/0004-637X/722/1/605](https://doi.org/10.1088/0004-637X/722/1/605)

Huang, Y., Liu, X. W., Yuan, H. B., et al. 2015, *MNRAS*, 449, 162, doi: [10.1093/mnras/stv204](https://doi.org/10.1093/mnras/stv204)

Hunt, E. L., & Reffert, S. 2023, *A&A*, 673, A114, doi: [10.1051/0004-6361/202346285](https://doi.org/10.1051/0004-6361/202346285)

Hunter, J. D. 2007, *Computing in Science & Engineering*, 9, 90, doi: [10.1109/MCSE.2007.55](https://doi.org/10.1109/MCSE.2007.55)

Hurley, J. R., Tout, C. A., & Pols, O. R. 2002, *MNRAS*, 329, 897, doi: [10.1046/j.1365-8711.2002.05038.x](https://doi.org/10.1046/j.1365-8711.2002.05038.x)

Irrgang, A., Wilcox, B., Tucker, E., & Schiefelbein, L. 2013, *A&A*, 549, A137, doi: [10.1051/0004-6361/201220540](https://doi.org/10.1051/0004-6361/201220540)

Jaschek, M., & Egret, D. 1982, in *IAU Symposium*, Vol. 98, *Be Stars*, ed. M. Jaschek & H. G. Groth, 261

Kahabka, P., Haberl, F., Payne, J. L., & Filipović, M. D. 2006, *A&A*, 458, 285, doi: [10.1051/0004-6361:20065490](https://doi.org/10.1051/0004-6361:20065490)

Kalari, V. M., Salinas, R., Saez-Carvajal, C., et al. 2025, arXiv e-prints, arXiv:2509.19286, doi: [10.48550/arXiv.2509.19286](https://doi.org/10.48550/arXiv.2509.19286)

Kennea, J. A., Coe, M. J., Evans, P. A., et al. 2021, *MNRAS*, 508, 781, doi: [10.1093/mnras/stab2632](https://doi.org/10.1093/mnras/stab2632)

Klement, R., Hadra, P., Rivinius, T., et al. 2021, *ApJ*, 916, 24, doi: [10.3847/1538-4357/ac062c](https://doi.org/10.3847/1538-4357/ac062c)

Klement, R., Schaefer, G. H., Gies, D. R., et al. 2022, *ApJ*, 926, 213, doi: [10.3847/1538-4357/ac4266](https://doi.org/10.3847/1538-4357/ac4266)

Kriz, S., & Harmanec, P. 1975, *Bulletin of the Astronomical Institutes of Czechoslovakia*, 26, 65

Lin, C.-C., Hou, J.-L., Chen, L., et al. 2015, *Research in Astronomy and Astrophysics*, 15, 1325, doi: [10.1088/1674-4527/15/8/015](https://doi.org/10.1088/1674-4527/15/8/015)

Liu, C., Fu, J., Shi, J., et al. 2020, arXiv e-prints, arXiv:2005.07210, doi: [10.48550/arXiv.2005.07210](https://doi.org/10.48550/arXiv.2005.07210)

Luo, A. L., Zhao, Y.-H., Zhao, G., et al. 2015, *Research in Astronomy and Astrophysics*, 15, 1095, doi: [10.1088/1674-4527/15/8/002](https://doi.org/10.1088/1674-4527/15/8/002)

Luo, A. L., Chen, J.-J., Hou, W., et al. 2018, in *Society of Photo-Optical Instrumentation Engineers (SPIE) Conference Series*, Vol. 10707, *Software and Cyberinfrastructure for Astronomy V*, ed. J. C. Guzman & J. Ibsen, 107072B, doi: [10.1117/12.2312433](https://doi.org/10.1117/12.2312433)

Maíz Apellániz, J., Negueruela, I., & Caballero, J. A. 2026, in *Encyclopedia of Astrophysics*, Vol. 2, 43–84, doi: [10.1016/B978-0-444-21439-4.00057-2](https://doi.org/10.1016/B978-0-444-21439-4.00057-2)

Marino, A., Yang, H. N., Coti Zelati, F., et al. 2025, *ApJL*, 980, L36, doi: [10.3847/2041-8213/ad9580](https://doi.org/10.3847/2041-8213/ad9580)

McMillan, P. J. 2017, *MNRAS*, 465, 76, doi: [10.1093/mnras/stw2759](https://doi.org/10.1093/mnras/stw2759)

McSwain, M. V., & Gies, D. R. 2005, *ApJS*, 161, 118, doi: [10.1086/432757](https://doi.org/10.1086/432757)

Mermilliod, J. C. 1982, *A&A*, 109, 48

Miroshnichenko, A. S., Pasechnik, A. V., Manset, N., et al. 2013, *ApJ*, 766, 119, doi: [10.1088/0004-637X/766/2/119](https://doi.org/10.1088/0004-637X/766/2/119)

Nagarajan, P., El-Badry, K., Reggiani, H., et al. 2025, arXiv e-prints, arXiv:2507.12532, doi: [10.48550/arXiv.2507.12532](https://doi.org/10.48550/arXiv.2507.12532)

Nedhath, S., Rani, S., Subramaniam, A., & Pancino, E. 2025, arXiv e-prints, arXiv:2506.08126, doi: [10.48550/arXiv.2506.08126](https://doi.org/10.48550/arXiv.2506.08126)

Negueruela, I., Simón-Díaz, S., de Burgos, A., Casasbuenas, A., & Beck, P. G. 2024, *A&A*, 690, A176, doi: [10.1051/0004-6361/202449298](https://doi.org/10.1051/0004-6361/202449298)

Neiner, C., de Batz, B., Cochard, F., et al. 2011, *AJ*, 142, 149, doi: [10.1088/0004-6256/142/5/149](https://doi.org/10.1088/0004-6256/142/5/149)

Ochsenbein, F. 1996, The VizieR database of astronomical catalogues, CDS, Centre de Données astronomiques de Strasbourg, doi: [10.26093/CDS/VIZIER](https://doi.org/10.26093/CDS/VIZIER)

Ochsenbein, F., Bauer, P., & Marcout, J. 2000, *A&AS*, 143, 23, doi: [10.1051/aas:2000169](https://doi.org/10.1051/aas:2000169)

pandas development team, T. 2020, *pandas-dev/pandas: Pandas*, latest Zenodo, doi: [10.5281/zenodo.3509134](https://doi.org/10.5281/zenodo.3509134)

Peters, G. J. 1983, *PASP*, 95, 311, doi: [10.1086/131164](https://doi.org/10.1086/131164)

Pols, O. R., Cote, J., Waters, L. B. F. M., & Heise, J. 1991, *A&A*, 241, 419

Porter, J. M., & Rivinius, T. 2003, *PASP*, 115, 1153, doi: [10.1086/378307](https://doi.org/10.1086/378307)

Poveda, A., Ruiz, J., & Allen, C. 1967, *Boletín de los Observatorios Tonantzintla y Tacubaya*, 4, 86

Reig, P., & Roche, P. 1999, *MNRAS*, 306, 100, doi: [10.1046/j.1365-8711.1999.02473.x](https://doi.org/10.1046/j.1365-8711.1999.02473.x)

Rivinius, T., Carciofi, A. C., & Martayan, C. 2013, *A&A Rv*, 21, 69, doi: [10.1007/s00159-013-0069-0](https://doi.org/10.1007/s00159-013-0069-0)

Rivinius, T., Klement, R., Chojnowski, S. D., et al. 2025, *A&A*, 694, A172, doi: [10.1051/0004-6361/202347275](https://doi.org/10.1051/0004-6361/202347275)

Rocha, D. F., Emilio, M., Labadie-Bartz, J., et al. 2025, arXiv e-prints, arXiv:2511.05761, doi: [10.48550/arXiv.2511.05761](https://doi.org/10.48550/arXiv.2511.05761)

Sana, H., de Koter, A., de Mink, S. E., et al. 2013, *A&A*, 550, A107, doi: [10.1051/0004-6361/201219621](https://doi.org/10.1051/0004-6361/201219621)

Secchi, A. 1866, *Astronomische Nachrichten*, 68, 63, doi: [10.1002/asna.18670680405](https://doi.org/10.1002/asna.18670680405)

Shao, Y., & Li, X.-D. 2014, *ApJ*, 796, 37, doi: [10.1088/0004-637X/796/1/37](https://doi.org/10.1088/0004-637X/796/1/37)

Shridharan, B., Mathew, B., Nidhi, S., et al. 2021, *Research in Astronomy and Astrophysics*, 21, 288, doi: [10.1088/1674-4527/21/11/288](https://doi.org/10.1088/1674-4527/21/11/288)

Skrutskie, M. F., Cutri, R. M., Stiening, R., et al. 2006, *AJ*, 131, 1163, doi: [10.1086/498708](https://doi.org/10.1086/498708)

Slettebak, A. 1985, *ApJS*, 59, 769, doi: [10.1086/191084](https://doi.org/10.1086/191084)

Tomsick, J. A., Heinke, C., Halpern, J., et al. 2011, *ApJ*, 728, 86, doi: [10.1088/0004-637X/728/2/86](https://doi.org/10.1088/0004-637X/728/2/86)

Tonry, J., & Davis, M. 1979, *AJ*, 84, 1511, doi: [10.1086/112569](https://doi.org/10.1086/112569)

Villaseñor, J. I., Sana, H., Bodensteiner, J., et al. 2025, arXiv e-prints, arXiv:2511.08675, doi: [10.48550/arXiv.2511.08675](https://doi.org/10.48550/arXiv.2511.08675)

Vioque, M., Oudmaijer, R. D., Schreiner, M., et al. 2020, *A&A*, 638, A21, doi: [10.1051/0004-6361/202037731](https://doi.org/10.1051/0004-6361/202037731)

Wang, L., Gies, D. R., & Peters, G. J. 2018, *ApJ*, 853, 156, doi: [10.3847/1538-4357/aaa4b8](https://doi.org/10.3847/1538-4357/aaa4b8)

Wang, L., Gies, D. R., Peters, G. J., et al. 2021, *AJ*, 161, 248, doi: [10.3847/1538-3881/abf144](https://doi.org/10.3847/1538-3881/abf144)

Wang, L., Li, J., Wu, Y., et al. 2022, *ApJS*, 260, 35, doi: [10.3847/1538-4365/ac617a](https://doi.org/10.3847/1538-4365/ac617a)

Wang, S., Zhang, H.-T., Bai, Z.-R., et al. 2021, *Research in Astronomy and Astrophysics*, 21, 292, doi: [10.1088/1674-4527/21/11/292](https://doi.org/10.1088/1674-4527/21/11/292)

Waters, L. B. F. M., Cote, J., & Pols, O. R. 1991, *A&A*, 250, 437

Wenger, M., Ochsenbein, F., Egret, D., et al. 2000, *A&AS*, 143, 9, doi: [10.1051/aas:2000332](https://doi.org/10.1051/aas:2000332)

Wolff, S. C., Strom, S. E., & Hillenbrand, L. A. 2004, *ApJ*, 601, 979, doi: [10.1086/380503](https://doi.org/10.1086/380503)

Wright, E. L., Eisenhardt, P. R. M., Mainzer, A. K., et al. 2010, *AJ*, 140, 1868, doi: [10.1088/0004-6256/140/6/1868](https://doi.org/10.1088/0004-6256/140/6/1868)

Zhang, B., Liu, C., & Deng, L.-C. 2020, *ApJS*, 246, 9, doi: [10.3847/1538-4365/ab55ef](https://doi.org/10.3847/1538-4365/ab55ef)

Zhang, B., Li, J., Yang, F., et al. 2021, *ApJS*, 256, 14, doi: [10.3847/1538-4365/ac0834](https://doi.org/10.3847/1538-4365/ac0834)

Zorec, J., Frémat, Y., Domiciano de Souza, A., et al. 2016, *A&A*, 595, A132, doi: [10.1051/0004-6361/201628760](https://doi.org/10.1051/0004-6361/201628760)

Zwicky, F. 1957, *Morphological astronomy*